Chlorophyll shading reduces zooplankton diel migration depth in a high-resolution physical biogeochemical model.

Mathieu A. Poupon[1,2], Laure Resplandy[1,3], Jessica Garwood[4], Charles Stock[5], Niki Zadeh[5], and Jessica Y. Luo[5]

[1]Department of Geosciences, Princeton University, Princeton, NJ, USA
[2]Atmospheric and Oceanic Sciences Program, Princeton University, Princeton, NJ, USA
[3]High Meadows Environmental Institute, Princeton University, Princeton, NJ, USA
[4]College of Earth, Ocean, and Atmospheric Sciences, Oregon State University, Corvallis, Oregon, USA
[5]NOAA Geophysical Fluid Dynamics Laboratory, Princeton, NJ, USA

Correspondence: Mathieu A. Poupon (mpoupon@princeton.edu)

Abstract. Zooplankton diel vertical migration (DVM) is critical to ocean ecosystem dynamics and biogeochemical cycles, by supplying food and injecting carbon to the mesopelagic ocean (200-800 m). The deeper the zooplankton migrate, the longer the carbon is sequestered away from the atmosphere and the deeper the ecosystems they feed. Sparse observations show variations in migration depths over a wide range of temporal and spatial scales. A major challenge, however, is to understand the biological and physical mechanisms controlling this variability, which is critical to assess impacts on ecosystem and carbon dynamics. Here, we introduce a migrating zooplankton model for medium and large zooplankton that explicitly resolves diel migration trajectories and biogeochemical fluxes. This model is integrated into the MOM6-COBALTv2 ocean physical-biogeochemical model, and applied in an idealized high-resolution (9.4 km) configuration of the North Atlantic. The model skillfully reproduces observed North Atlantic migrating zooplankton biomass and DVM patterns. Evaluation of the mechanisms controlling zooplankton migration depth reveals that chlorophyll shading reduces by 60 meters zooplankton migration ~~depth~~ depths in the subpolar gyre compared with the subtropical gyre, with pronounced seasonal variations linked to the spring bloom. Fine-scale spatial effects (<100 km) linked to eddy and frontal dynamics can either offset or reinforce the large-scale effect by up to 100 meters. This could imply that for phytoplankton-rich regions and filaments, which represent a major source of exportable carbon for migrating zooplankton, ~~their~~ high-chlorophyll content contributes to reducing zooplankton migration depth and carbon sequestration time.

1 Introduction

The diel vertical migration (DVM) of zooplankton is the largest synchronized movement of ~~organism~~ organisms on Earth, with major implications for the ocean ecosystem dynamics and biogeochemical cycles (Hays et al., 1997; Steinberg et al., 2002; Bianchi et al., 2013b). Every day at dawn, after spending the night feeding, half of the world's zooplankton biomass leaves the surface ocean for deeper waters, where it remains before swimming back to surface waters at dusk (Klevjer et al., 2016). Migrating zooplankton shape biogeochemical cycles by consuming organic matter in the surface waters and respiring

or excreting some of it deeper down, sequestering carbon away from the atmosphere, and potentially accounting for 10-30% of the biological carbon pump (Steinberg et al., 2000; Boyd et al., 2019; Aumont et al., 2018; Archibald et al., 2019; Nowicki et al., 2022). This efficient vertical transport of organic matter by DVM influences the depth at which nutrients are regenerated

25 (Steinberg et al., 2002; Longhurst and Glen Harrison, 1988; Bianchi et al., 2013b, 2014), and intensifies respiration and oxygen depletion at the upper margin of oxygen minimum zones (around 200-500 meters deep, Bianchi et al., 2013a; Aumont et al., 2018). DVM also contributes to structuring trophic interactions by providing energy to mesopelagic ecosystems (Kelly et al., 2019), triggering cascade migration of lower trophic levels (Bollens et al., 2011) and altering the foraging performance of visual predators such as fish and marine mammals by hiding in the dark (Benoit-Bird and Moline, 2021; Chambault et al.,

30 2024).

Zooplankton migration depth is a key factor for understanding the impact of DVM on carbon and oxygen cycles, and ecosystem dynamics. The deeper migrating zooplankton egest, excrete or respire material from the surface, the deeper nutrients are regenerated and oxygen is consumed, and the longer the carbon they release is sequestered away from the atmosphere (Boyd et al., 2019). The fecal pellets they egest can also serve as a food source for ecosystems at that depth and below (Kelly et al.,

35 2019). Migration depth observations vary by several hundred meters over multiple spatial and temporal scales. For example, at fine spatial scales, Powell and Ohman (2015) have shown that zooplankton migrate 200 meters deeper on one side of a 20 km-wide front than on the other. At the basin scale, Bianchi et al. (2013a) showed that zooplankton swam about 200 meters deeper in the subtropical gyre than in the North Atlantic subpolar gyre. Temporally, Omand et al. (2021) have shown that migration depth can fluctuate up to 50 meters within a single day, while Hobbs et al. (2021) have documented the existence

40 of a seasonal cycle in zooplankton migration depth. However, the mechanisms controlling zooplankton diel vertical migration patterns and their biogeochemical consequences are still poorly quantified (Bandara et al., 2021).

Light is often considered the main cue that determines zooplankton migration timing and depth (Brierley, 2014). The most common hypothesis, known as the "preferendum hypothesis", states that migrating organisms modify their depth when irradiance changes, to remain in a preferred light level, or isolume (Ewald, 1910; Michael, 1911; Russell, 1927). This behavior keeps

45 them hidden from visual predators (Zaret and Suffern, 1976). Numerous studies supporting this hypothesis have shown that factors modifying irradiance at the ocean surface, such as sunlight, moonlight, cloud cover, ice cover or eclipses (Strömberg et al., 2002; Haren and Compton, 2013; Last et al., 2016; Omand et al., 2021; Flores et al., 2023), or in the water column, such as water transparency and chlorophyll content could modify the migration depth (Dickson, 1972; Powell and Ohman, 2015; Hobbs et al., 2021). Migration timing can further be modified by other exogenous factors such as predation pressure (Ohman

50 et al., 1983; Lass and Spaak, 2003; Bollens and Frost, 1989) or food availability (Pijanowska and Dawidowicz, 1987; Beklioglu et al., 2008), or endogenous ones such as circadian rhythms (Harris, 1963). Similarly, migration depth can also be modified by environmental exogenous parameters such as low oxygen concentrations (Bianchi et al., 2013a), temperature or salinity (Kimmerer et al., 1998; Glaholt et al., 2016), and endogenous ones such as zooplankton size (Ohman and Romagnan, 2016). However, the limited number of observations makes it challenging to disentangle and quantify the individual contribution of

55 these different factors on migration depth's spatial and temporal variations.

Although numerical models can provide further insights, modeling diurnal vertical migration poses several challenges. First, migration is affected by several physical, chemical and biological variables (e.g. light, oxygen concentration, food availability and predation exposure), requiring models that capture these complex processes, as well as a realistic representation of zooplankton physiology key to biogeochemical impacts (e.g. egestion, excretion, respiration, growth and mortality rates). Second, diel vertical migration is a rapid process, where zooplankton reach migration velocities ranging from 3 to 15 cm.s^{-1} (Bianchi and Mislan, 2016), and is modulated at various temporal and spatial scales. Modeling such fast zooplankton vertical migration over a wide period and ocean area at high spatial and temporal resolution is therefore limited by computational cost. Existing models fail at capturing this complexity. One-dimensional vertical models explicitly represent zooplankton physiology and migration trajectory based on isolumes (Bianchi et al., 2013b; Nocera et al., 2020), or taking into account exposure to food and predators to maximize fitness (Pinti et al., 2019), but do not represent ocean circulation. Conversely, three-dimensional global biogeochemical models capturing ocean circulation represent vertical migration in parameterized form, where the biogeochemical fluxes created are distributed around a migration depth determined by an isolume or oxygen threshold (Aumont et al., 2018; Archibald et al., 2019; Nowicki et al., 2022). In this case, migration trajectories are not explicitly modeled and the seasonal cycle is not always represented. Furthermore, none of these modelling approaches capture the effect of fine-scale dynamics (< 100 km), such as fronts and eddies, on zooplankton migration patterns. To improve our understanding of the impact of DVM on biogeochemical and ecosystem dynamics, we need to develop models explicitly representing both the migration trajectories and physiology of migrating zooplankton, as well as their interactions with the environment over a wide range of space and time scales.

In this study, we develop a migrating zooplankton module and fully ~~integrated~~ integrat it into a coupled physical-biogeochemical model of the North Atlantic. This model includes a range of biological and physical mechanisms that affect zooplankton migration patterns and physiology over multiple spatial and temporal scales. We use an idealized double gyre high-resolution configuration of the North Atlantic, built using an ocean circulation model (Adcroft et al., 2019) coupled with a biogeochemical model (Stock et al., 2020). Our idealized configuration replicates the characteristic biophysical dynamics of the subtropical and subpolar gyres, their seasonal cycle and fine-scale dynamics. Our migrating zooplankton module includes two migrating zooplankton size classes (medium, large) and explicitly represents their migration ~~trajectory~~trajectories, controlled by light, oxygen concentration, size and prey distribution. Zooplankton physiology is also explicitly modeled and depends on environmental factors (e.g. temperature) and individual factors (e.g. zooplankton feeding activity or swimming). We show that our zooplankton migration model reproduces the contrasts in biomass, timing and migration depth of migrating zooplankton observed in the North Atlantic. We identify and quantify the mechanisms responsible for modulating the migration depth of zooplankton in the North Atlantic (surface irradiance, chlorophyll shading and ocean transport). We explore their variation across seasons, biomes (subtropical vs subpolar) and spatial scales (gyre scale vs fine scales), and show that chlorophyll shading is the dominant process structuring migration depth at all these scales.

2   Materials and Methods

We develop an idealized double gyre ocean model reproducing the North Atlantic biophysical ocean dynamics (Sect. 2.1). Our
model is coupled to the biogeochemical module (COBALTv2), and extended in this study to integrate two vertically migrating
zooplankton (COBALTv2-DVM, Sect. 2.3). Our new module represents realistic migration ~~trajectory~~ trajectories (Sect. 2.3.1),
visual predation (Sect. 2.3.2) and zooplankton physiology (Sect. 2.3.3). We also develop a framework to quantify the processes
modulating zooplankton migration depth (e.g., irradiance seasonality, chlorophyll shading effect at large and fine ~~scale~~scales,
vertical transport, see Sect. 2.4).

2.1   Idealized double gyre experiment

2.1.1   Configuration

We use an idealized double gyre reproducing a biophysical dynamics characteristic of the North Atlantic Ocean, including a
low-productivity subtropical gyre and a ~~highly productive~~ high-productivity subpolar gyre separated by a jet analogous to the
Gulf Stream, as well as a deep winter convection region (Fig. 1). Idealized double gyre models are useful tools to examine the
influence of gyre circulation and eddies on ventilation (Marshall et al., 2002; Radko and Marshall, 2003; Henning and Vallis,
2004), and phytoplankton and biological carbon pump dynamics (Lévy et al., 2015; Resplandy et al., 2012, 2019; Couespel
et al., 2021).

Here, the double gyre model was built using the Modular Ocean Model version 6 (MOM6 Adcroft et al., 2019). The domain
is a square of 3570 km side length, 4000 m depth, 9 km horizontal resolution, 2-5 m vertical resolution between 0 and 100 m
depth, 10-100 m between 100 and 1000 m depth and up to 250m below. The configuration is centred around 40°N and under
the β-plane approximation ($f_0 = 9.35 \times 10^{-5}$ s^{-1}, $\beta = 1.75 \times 10^{11}$ m^{-1} s^{-1}). The four vertical boundaries are solid imper-
meable walls preventing any lateral exchanges. This physical model is coupled to the Carbon, Ocean Biogeochemistry and
Lower Trophics biogeochemical module version 2 (COBALTv2 Stock et al., 2020). COBALTv2 includes 33 biogeochemical
tracers, such as the main nutrients (e.g. nitrogen, phosphorus, iron, silica) and a planktonic ecosystem. The original version
of COBALTv2 included 3 phytoplankton and 3 non-migrating zooplankton, to which we added 2 migrating zooplankton (see
Sect. 2.3). Vertical movement was simulated with an implicit solution of the advection-diffusion equation generalized to han-
dle upward and downward swimming. The resulting tridiagonal matrix was solved using the algorithm described in Press
(2007). Each year, the double gyre is forced by the same idealized ~~atmospheric zonally uniform~~ zonally uniform atmospheric
climatology detailed below. Further details on the model parameters are in the supplementary material (Table S1).

2.1.2   Forcings

The ocean surface is forced with an idealized wind field (Fig. A1a). The zonal wind stress follows a sinusoidal profile, minimal
at the northern and southern boundaries of the domain (-0.1 N m^{-2}), maximal at 40° N (0.1 N m^{-2}) and varying by 10%
in amplitude according to a seasonal cycle (e.g., higher values in ~~december~~December). The meridional wind stress is zero.
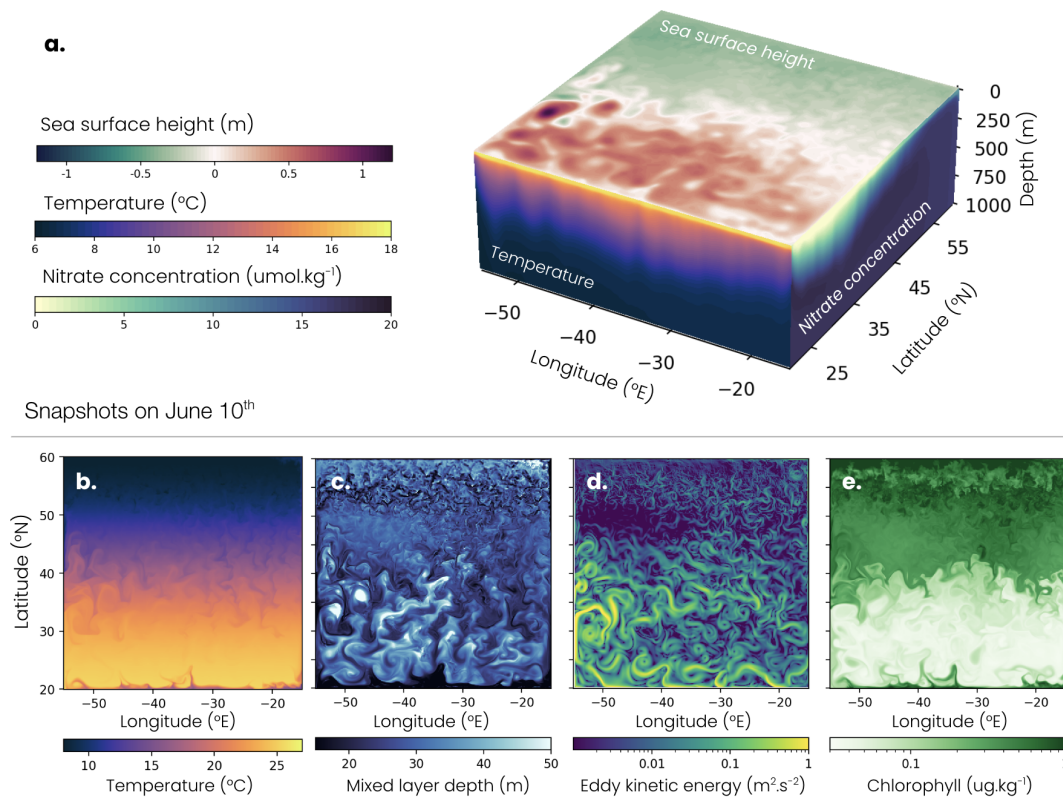
Figure 1. Double gyre set-up: June 10th snapshot of (a) sea surface height (top) and depth sections of temperature at 20° N (front) and nitrate concentration at -15° E (right); (b) sea surface temperature, (c) mixed layer depth, (d) eddy kinetic energy and (e) surface chlorophyll concentration.

The radiative forcing is derived from the ERA5 atmospheric reanalysis (Hersbach et al., 2020) averaged over the 1979-2022 period (Fig. A1g). The temporal resolution of ERA5 (1h) accurately resolves the daily cycle of irradiance required for vertical migration modeling. The forcing is calculated as the zonal mean over a thin band of 2° longitude located in the middle of the North Atlantic (longitude = -35° E to -33° E, latitude = 20° N to 60° N), which avoids the daily light cycle being skewed by the time difference between the east and west Atlantic basin. This radiative forcing, like all the other surface forcings, is temporally synchronous across the whole basin on daily time scales and linearly interpolated every 5 minutes, between available forcing values. This resolution enables our model to accurately represent the mean daily light cycle, although it may not perfectly resolve the crepuscular period, when zooplankton begin to migrate. The other physical atmospheric forcings (pressure, temperature, precipitation, humidity) are derived from the JRA55-do atmospheric reanalysis (Tsujino et al., 2018) with a 3-h time resolution averaged over the period 1958-2020 (Fig. A1b-f). They are calculated as the zonal mean over a wider region covering most of the North Atlantic Ocean (longitude = -60° E to -20° E, latitude = 20° N to 60° N). Precipitation from JRA55-do is adjusted to ensure that the same mass of precipitation is received by the double gyre as by the North Atlantic

Ocean and a mass restoration flux is applied at the surface to ensure its conservation (Fig. A1e). Iron and lithogenic material deposition (Fig. A1h-i) are calculated as the zonal mean of the last 30 years of a GFDL-ESM4 pre-industrial control simulation spanning from 1850 to 2014 (Dunne et al., 2020), over the same band as the physical forcings.

2.1.3 Initial state and spin-up

135 Temperature and salinity as well as nitrate, oxygen, phosphate, silica concentrations are initialized uniformly zonally using the World Ocean Atlas 2018 zonal mean (Boyer et al., 2018) over the region delimited by -60° E to -20° E and 20° N to 60° N. Similarly, alkalinity and dissolved inorganic carbon are initialized from GLODAPv2 (Olsen et al., 2020) and the rest of the biogeochemical tracers are initialized from the GFDL-ESM4 simulation described above, all using zonally averaged fields in the same region. The model is first spun-up for 1000 years at coarse resolution (85 km) and then run for 25 years at a
140 eddy-permitting resolution (9 km, Table S1). This paper focuses on the last 5 years at 9 km resolution

2.2 Observations

To evaluate the biophysical dynamics simulated in the model, we use multiple observational data products. The nutrient concentration, temperature and salinity ~~used~~ are taken from the World Ocean Atlas 2018 (Garcia et al., 2019, Fig. A2), the mixed layer depth from a compilation of hydrographic sections between 1941 and 2002 from de Boyer Montégut et al. (2004), sur-
145 face chlorophyll concentration from a combination of satellite observations between 1997 and 2020 from Sathyendranath et al. (2019) and net primary productivity is derived from Moderate-Resolution Imaging Spectroradiometer (MODIS) measurements between 2002 and 2023 processed by three algorithms (Eppley, CbPM and CAFE Behrenfeld and Falkowski, 1997; Westberry et al., 2008; Silsbe et al., 2016).

The biomass of migrating zooplankton is evaluated using estimates derived from LIDAR observations between 2007 and
150 2019 (Behrenfeld et al., 2019) and net samples at the Bermuda Atlantic Time Series (BATS) station between 1994 and 2010 (Steinberg et al., 2012). We also use estimates of migration depth and time spent at depth by migrating zooplankton derived from acoustic doppler current profiler (ADCP) measurements taken between 1990 and 2010 and compiled by Bianchi and Mislan (2016).

2.3 ~~Model biome definition and biogeochemical evaluation~~

155 ~~Our model reproduces the characteristic physical and biogeochemical dynamics of four biomes of the North Atlantic: a low-productivity subtropical gyre, a productive subpolar gyre, an energetic jet in between with intense mesoscale eddy activity, and a deep winter convection region in the northern part of the domain (Fig. 1, Fig. 5 and Fig. A2). The subtropical, subpolar and jet biomes are defined by thresholds of annual surface chlorophyll concentration (0.15~~ Note that these observations are particularly rare and challenging to collect, and ~~0.35 mg m^{-3}), as used in previous studies (Resplandy et al., 2012, 2019). The~~
160 ~~convecting region is identified as a subregion of the subpolar region, using the 200-meter threshold on the annual mean mixed layer depth. Our main conclusions are not sensitive to these thresholds. Note that the wind creates an upwelling along the wall~~

at the southern boundary and stimulates ocean productivity with annual mean chlorophyll concentrations higher than 0.35 mg m^{-3} (Fig. 5d). This upwelling, representative of the equatorial dynamics occurring further south in nature, is excluded from the analysis using the chlorophyll thresholds given above. may be subject to measurement method bias. Acoustic methods can be biased towards highly sound-scattering animals (Flagg and Smith, 1989), net measurements capture neither animals smaller than the mesh, nor larger ones able to avoid the net, while LIDAR data can be biased towards larger plankton and miss biomass capture of smaller plankton.

Map of annual mean (a,b) mixed layer depth (MLD), (d,e) surface chlorophyll concentration and (h,i) migrating zooplankton biomass in (a,d,h) the double gyre model and (b,e,i) observation-based data products. The subtropical, jet and subpolar biomes are delimited by solid black lines (mean surface chlorophyll concentration = 0.15 and 0.35 $mg\ m^{-3}$), while the subpolar and convective biomes are delimited by a dashed line (mean MLD = 200 m, see Methods). Mean seasonal cycle of (c) MLD, (f) net primary productivity and (j) migrating zooplankton biomass in the subtropical biome (orange) and the subpolar biome (blue) in the the double gyre model (solid lines) and observation-based products (dashed lines). Shading and error bars correspond to two standard deviations around the average. Orange star in (i) indicate the Bermuda Atlantic Time-series Study (BATS). See Sect. 2.2 for observational product details.

The mean biophysical conditions and seasonal cycle simulated within the biomes are similar to those observed in the ocean. In both observations and model, the subtropical anticyclonic gyre (elevated sea surface height, Fig. 1a) is oligotrophic at the surface, with nitrogen concentrations below 1 μmolN kg^{-1}, and phosphorus concentrations below 0.1 μmolP kg^{-1} in the first 100 meters (Fig. A2a-d). The model also reproduces the observed stratification throughout the year, with a mixed layer varying between 30 and 60 m seasonally (Fig. 5a-c), strongly limiting the supply of nutrients to the surface. Consequently, net primary productivity in the subtropical gyre is low (between 170 and 250 mgC m^{-2} d^{-1} on average in model and observation-based estimates) and varies little seasonally (Fig. 5d-f). In contrast, the subpolar cyclonic gyre (depressed sea surface height) is a nutrient-rich environment. Nitrate concentrations range from 8 to 17 μmolN kg^{-1} in the top 100 meters, and phosphate concentrations from 0.3 to 0.8 μmolP kg^{-1} (Fig. 1a, Fig. A2a-d) in both observations and model. This is partly due to high seasonality, with a modeled mixed layer averaging 140 m in winter (125 m in observations, Fig. 5c), bringing nutrients to the surface. Consequently, netprimary productivity in the subpolar gyre is high and seasonally marked (Fig. 5f). It increases from January onwards, peaks in May (920 mgC m^{-2} d^{-1} in model, 650-930 mgC m^{-2} d^{-1} in observations) and falls back below 500 mgC m^{-2} d^{-1} at the end of summer.

Finally, at the northern boundary, the wind creates a downwelling and a deep convecting water column characterized by winter mixed layers exceeding 1000 meters (Fig. 5a). These deep convection events can be considered as representative of ocean dynamics occurring further north in the Atlantic Ocean, such as the Irminger and the Labrador Seas (Fig. 5b). These convection events bring a high concentration of nutrients to the surface (>12 μmolN kg^{-1} and $>$ 0.7 μmolP kg^{-1}, Fig. 1a, Fig. A2a-d) and sustain a biome productivity of 420 mgC m^{-2} d^{-1} on annual average, reaching up to 1250 mgC m^{-2} d^{-1} in spring.

These large-scale dynamics are locally modulated by fine-scale structures such as eddies and fronts (Fig. 1b-e). The jet hosts the most energetic fine-scale dynamics (Fig. 1d, Fig. A3), because it is unstable and therefore induces eddy formation.

~~Many eddies are present in the subtropical gyre, since the horizontal resolution of the model is sufficient to resolve mesoscale dynamics (>100 km). Conversely, in the subpolar gyre, the resolution is not sufficient to fully resolve these eddies, leading to less coherent and more filamentary turbulent structures. As we will show in this study, these features introduce variability in~~ 200 ~~the gyre and seasonal dynamics and are key to understand zooplankton migration depth variability.~~

2.3 Migrating zooplankton model

We developed the COBALTv2-DVM module by adding two migrating zooplankton to the pre-existing COBALTv2 biogeochemical module (Stock et al., 2020). These migrating zooplankton are the same as the medium (0.2-2 mm) and large (2-20 mm) zooplankton of COBALTv2 in terms of prey preferences and density-dependent higher trophic level predator losses. 205 However, they perform diel vertical migration (2.3.1), enabling them to escape visual predation (2.3.2). They also have a compartmentalized physiology that temporally decouples ingestion, digestion, respiration and growth (2.3.3), to realistically represent the matter fluxes which differ when zooplankton feed at the surface and when they dive, as highlighted by the work of Bianchi et al. (2013b).

2.3.1 Migration model

210 The migration trajectory of zooplankton is controlled by the light intensity, oxygen concentration and vertical distribution of its prey (Fig. 2a). Migration is assumed to be solely vertical and is controlled by the vertical migration velocity (w).

During the day, migrating zooplankton dive following an isolume, i.e. a preferred light intensity level (I_{iso}, medium: I_{iso} = 10^{-3} W m^{-2}, large: I_{iso}= 10^{-4} W m^{-2}). As a result, large zooplankton dive deeper than medium zooplankton. The migration speed $w(z)$, positive downward, is close to the maximum swimming speed (w_0) away from the isolume and starts to decrease, 215 according to a Monod equation, when it approaches about 50 ~~meters~~ m from its isolume:

$$w(z) = \eta_{iso}(z) w_0 \frac{|\frac{1}{K_{Blue}} \ln(\frac{I_{iso}}{I(z)})|}{K_{dz} + |\frac{1}{K_{Blue}} \ln(\frac{I_{iso}}{I(z)})|} \tag{1}$$

With ~~K$_{blue}$~~ K_{blue} = 0.0232 m^{-1} the light attenuation coefficient for optically pure seawater (Manizza et al., 2005), ~~K$_{dz}$~~ K_{dz} = 50 m the half-saturation distance, ~~I(z)~~ $I(z)$ the irradiance at depth z, and w_0 the maximum migration velocity determined from observations (medium w_0 = 6 cm s^{-1}, large: w_0 = 8 cm s^{-1}, Fig. A7). ~~The model also includes a migration depth~~ 220 ~~limitation by an oxygen threshold, set to 10 μmolO$_2$ kg^{-1}, similarly to Aumont et al. (2018). However, this limitation is not utilized in our simulation as oxygen concentrations are higher than 10 μmolO$_2$ kg^{-1}, and therefore do not limit migration. The sensitivity of the results to the migration model parameters (w_0, I$_{iso}$, K$_{dz}$) is assessed by varying their values by ± 50% (see Fig. B3).~~

~~At~~ $\eta_{iso}(z)$ is 1 or -1 depending on the zooplankton position (z) and controls the migration direction. When zooplankton 225 are above the isolume depth ($z < z_{iso}$), $\eta_{iso}(z) = 1$ and zooplankton swim downwards. When the zooplankton is below the isolume, e.g. because the isolume rises at dusk or is absent at night, migrating zooplankton return to the surface to feed. To
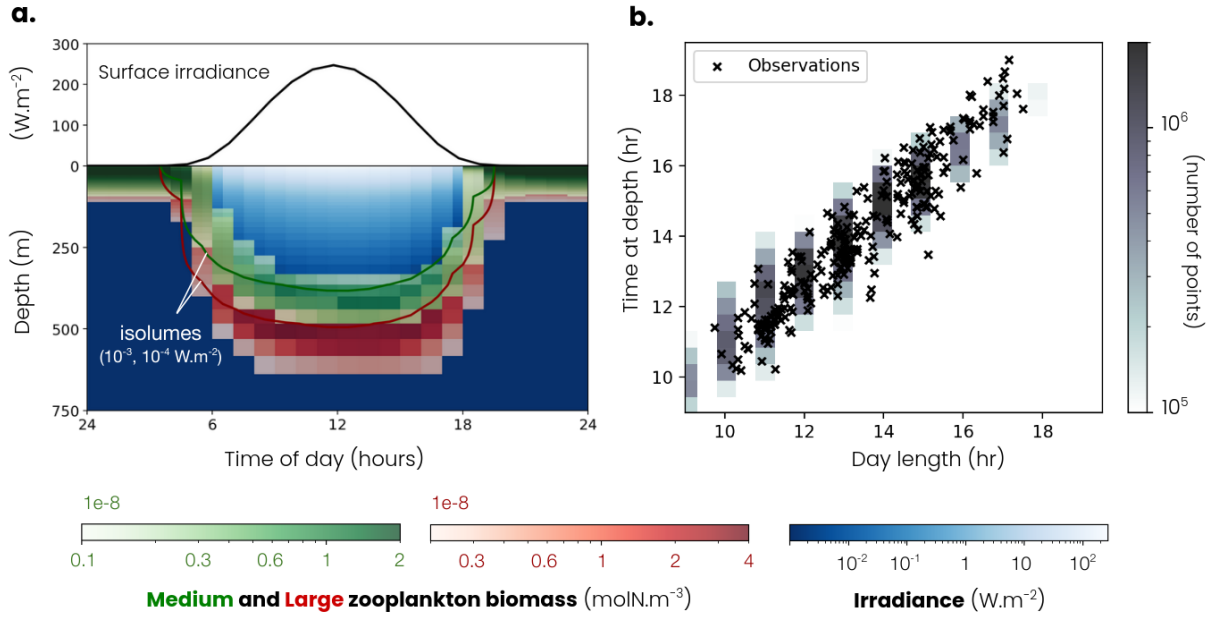
Figure 2. (a) Top of panel - Mean daily surface irradiance cycle (black line). Bottom of panel - Mean daily cycle of migrating zooplankton biomass (medium: green color fill, large: red color fill), migrating zooplankton isolume depth (medium: green line, isolume = 10^{-3} W m^{-2}, large: red line, isolume = 10^{-4} W m^{-2}) and irradiance (blue color fill). (b) Time spent at depth by migrating zooplankton as a function of day length in observations (cross) and model (distribution of model points shown by grey color fill).

reproduce foraging behavior, migrating zooplankton distributions are redistributed according to the distribution of its ~~preys, using~~prey and $\eta_{iso}(z)$ can be 1 or -1, depending on:

$$ZooExcess(z) = \int\limits_{0}^{z} \left(\frac{Z(z')}{\overline{Z}} - \frac{P(z')}{\overline{P}} \right) dz' \qquad (2)$$

230   Where $Z(z')$ and $P(z')$ are the concentrations of zooplankton and its prey at depth z'. $\overline{Z}$ and $\overline{P}$ ~~is~~ are their mean concentration over the entire water column. At a given depth z_0, if $ZooExcess(z) > 0$, the zooplankton ~~is~~are in relative excess with respect to ~~its~~their prey between the surface and this depth. Therefore, zooplankton dive (~~$w(z) = w_0$~~$\eta_{iso}(z) = 1$) to restore the balance. If $ZooExcess(z) < 0$, the zooplankton ~~is~~are in relative deficit to ~~its~~their prey. Therefore, zooplankton rise to fill this imbalance (~~$w(z) = -w_0$~~$\eta_{iso}(z) = -1$). Note that if the zooplankton below the isolume rises and reaches it, the zooplankton

235   remains at the isolume depth, since its migration velocity becomes zero ($w(z = z_{iso}) = 0$).

The model also includes a migration depth limitation by an oxygen threshold, set to 10 μmolO$_2$ kg^{-1}, similarly to Aumont et al. (2018), However, this limitation is not utilized in our simulation as oxygen concentrations are higher than 10 μmolO$_2$ kg^{-1}, and therefore do not limit migration. The sensitivity of the results to the migration model parameters (w_0, I_{iso}, K_{dz}) is assessed by varying their values by $\pm$ 50% (see Fig. B3).

<234054 />

2.3.2 Visual predation model

In the ocean, zooplankton migrate vertically to escape visual hunting predators. To represent this competitive advantage of migrating zooplankton over non-migrating, we implemented the visual predation model derived by Bianchi et al. (2013b) in COBALTv2-DVM. In this model, a fraction of the predation rate of top predators (I_{HP}) on zooplankton (Z), corresponding to visual predation, increases with irradiance ($I(z)$, Fig. A8):

$$I_{HP} = I_{HP}^{max} \cdot \frac{Z}{K_Z + Z} \cdot \left((1 - \alpha) + \alpha \frac{I(z)}{\left(\frac{K_Z}{K_Z + Z}\right) \cdot K_{irr} + I(z)} \right) \qquad (3)$$

Where I_{HP}^{max} is the maximum predation rate of top predators, which varies with temperature and oxygen concentration, $K_Z = 1.25\ \mu\text{molN kg}^{-1}$ is the half saturation constant for prey density dependence, $\alpha = 0.9$ is the maximum predation fraction due to visual predators and $K_{irr} = 10^{-1}\ \text{W m}^{-2}$ is the half saturation response for light limitation. At the surface during the day, irradiance is sufficient ($I(z) \gg K_{irr}$) and does not limit visual predation: $I_{HP}(z) \approx I_{HP}^{max} \frac{Z}{K_Z + Z}$. During the night or at depth, the absence of light ($I(z) \ll K_{irr}$) inhibits visual predation and limits the predation rate to 10% of its maximum value: $I_{HP}(z) \approx (1 - \alpha) I_{HP}^{max} \frac{Z}{K_Z + Z}$.

2.3.3 Zooplankton physiological model

To reproduce realistic biogeochemical fluxes produced by zooplankton digestion, respiration, and death, we developed a six-compartment model. The model, inspired by that of Bianchi et al. (2013b), was extended to represent phosphate, iron and silica dynamics as well as the thermal dependence of the gut clearing rate. The model represents nitrogen (N^{gut}), phosphorus (P^{gut}), iron (Fe^{gut}) and silica (Si^{gut}) in the zooplankton gut, as well as nitrogen metabolites (N^{metab}) and nitrogen body biomass (N^{body}, Fig. 3).

First, zooplankton fill their guts with the nitrogen, phosphorus, iron and silica contained in their prey. The gut content ($X^{gut} = N^{gut}$, P^{gut}, Fe^{gut} or Si^{gut}) is cleared by egestion and assimilation following an e-folding timescale ranging from 15 minutes to 3 hours, depending on water temperature (Fig. A6).

$$\frac{\partial X^{gut}}{\partial t} = ingestion_X - k^{clear} \cdot X^{gut} \qquad (4)$$

$$k^{clear} = k_0^{clear} + k_T^{clear} \cdot (T - T_0) \qquad (5)$$

Where $T_0 = 0\ °\text{C}$, and the coefficients $k_0^{clear} = 8\ \text{d}^{-1}$, $k_T^{clear} = 4.32\ °\text{C}^{-1}\ \text{d}^{-1}$ are derived from a linear regression on a set of digestion rate observations for different temperatures (Irigoien, 1998). The ingestion rate ($ingestion_X$) depends on prey and zooplankton abundance, and increases exponentially with temperature (see Stock et al., 2014).

Following the same ratios as the non-migrating zooplankton, 30% of the nitrogen and phosphorus consumed are egested as organic matter (medium: 70% of the egestion as particulate sinking detritus and 30% in dissolved form, large: 100% of the egestion is detritus). The remaining 70% of the consumption are assimilated ($assimilation_{N|P}$) as metabolites at a ratio of

<934054 />
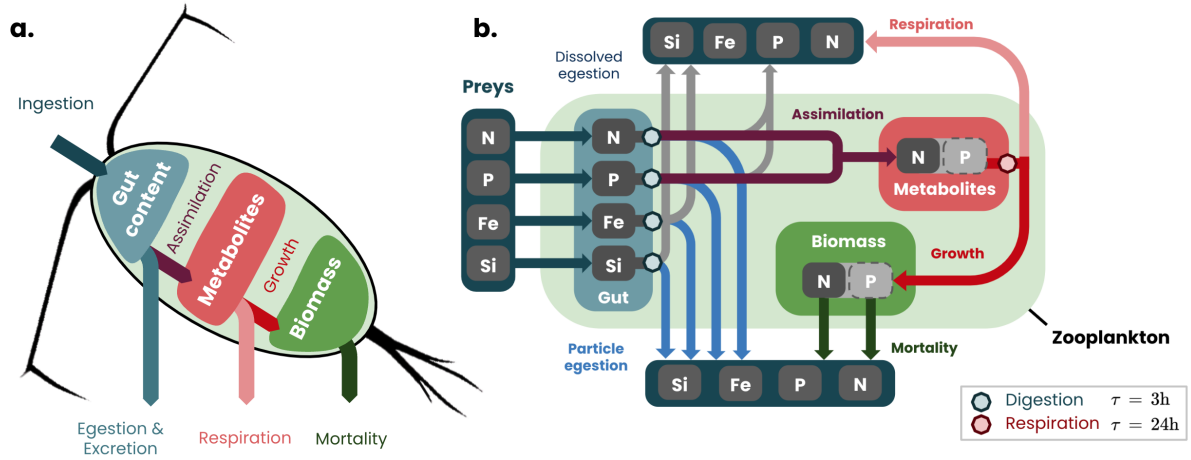
Figure 3. Migrating zooplankton model COBALTv2-DVM: (a) simplified and (b) detailed schemes of biogeochemical fluxes and stocks. The gut content (blue box) is filled by ingestion and cleared by egestion, excretion and assimilation, occurring between 10 min and 3 hours after ingestion. The metabolite pool (light red box) is filled through assimilation and used for zooplankton growth and respiration, occurring throughout the day. The biomass (green box) accumulates through growth and declines through mortality.

$N : P = 1 : 16$, allowing the metabolic content to be modeled with a single tracer (N^{metab}). Nitrogen and phosphorus in excess compared to this ratio is egested as dissolved inorganic form (NH$_4$ and PO$_4$, respectively). Silica and iron are totally egested, 30% as organic matter (medium: 70% as particulate sinking detritus and 30% in dissolved form, large: 100% as detritus) and the rest ~~in~~ as dissolved inorganic matter. These ratios are chosen to be the same as those used by Stock et al. (2014, 2020) for non-migrating zooplankton.

Metabolites are consumed by metabolic reactions ($metabolism$), i.e. the sum of anabolic ($growth$, through organic biomass synthesis) and catabolic ($respiration$, production of energy necessary for the functioning of the organism) reactions according to an e-folding timescale of 24h (~~k^{resp}~~ k^{resp} = 1 d^{-1}):

$$\frac{\partial N^{metab}}{\partial t} = assimilation_{N|P} - metabolism \tag{6}$$

$$metabolism = growth + respiration = k^{resp} \cdot N^{metab} \tag{7}$$

The $respiration$ flux is the sum of three terms. The first ~~one~~ term is the respiration of metabolites to maintain the vital functions ($respiration_{basal}$), the second ~~one~~ term covers the energetic needs of assimilation and digestion ($respiration_{feeding}$) and the last ~~one~~ term is linked to swimming ($respiration_{swim}$):

$$respiration = respiration_{basal} + respiration_{feeding} + respiration_{swim} \tag{8}$$

$$respiration_{basal} = \mu_{basal} \cdot N^{body} \tag{9}$$

$$respiration_{feeding} = \gamma^{resp} \cdot k^{resp} \cdot N^{metab} \tag{10}$$

$$respiration_{swim} = \frac{w}{w^{ref}} \cdot \mu_{basal} \cdot N^{body} \tag{11}$$

Where μ_{basal} is the basal respiration rate of zooplankton, which increases exponentially with temperature (see Stock et al., 2014), γ^{resp} is the fraction of metabolic flux used to cover assimilation and digestion processes, w is the migration velocity of zooplankton, and w^{ref} is the reference velocity for adjusting the energy cost of swimming. The linear relationship between respiration ($respiration_{swim}$) and swimming velocity was proposed by Torres and Childress (1983) and previously used in the model developed by Bianchi et al. (2013b). Biomass production by anabolism ($growth$) is equal to the difference between the metabolic ($metabolism$) and catabolic ~~fluxes~~ ($respiration$) fluxes. If this difference is positive, the biomass increases. If it is negative, part of the zooplankton does not have the metabolic resources to ensure its catabolic needs. This part of the zooplankton dies and its biomass is transformed into sinking detritus.

Most of the model parameters are directly derived from the literature (such as digestion rate - k_0^{clear} and its temperature sensitivity - k_T^{clear}) or were already part of the pre-existing COBALTv2 model. Four parameters (basal respiration rate - μ_{basal}, grazing rate, reference swimming speed - w^{ref}, maximum predation fraction due to visual predators - α) were adjusted using 14 sensitivity experiments (see Fig. A5). We selected the parameter values to match the observed fraction and biomass of migrating zooplankton (see Fig. 5h, Fig. A5). Note that this complex physiological parameterization is only applied to migrating zooplankton, in order to separate fluxes temporally and therefore spatially. Without migration, this parameterization would give similar results to non-migrating zooplankton, on a daily average.

2.4 Migration depth analysis framework

In this section, we present a framework to investigate which processes control zooplankton migration depth. First, we isolate the effects of surface irradiance, chlorophyll shading, and ocean transport (2.4.1). Then, we separate their contributions according to different spatial and temporal scales (2.4.2).

2.4.1 Migration depth decomposition

We decompose the migration depth (z_{mig}) as the sum of three terms (Fig. 4) controlled respectively by irradiance in transparent water ($z_{iso,tw}$), variations in chlorophyll shading (Δz_{chl}) and variations in ocean circulation vertical transport (Δz_{circ}):

$$z_{mig} = z_{iso,tw} + \Delta z_{chl} + \Delta z_{circ} \tag{12}$$

$z_{iso,tw}$ is the isolume depth in transparent water. It represents the depth at which the isolume would be if only the effects of light absorption by water molecules were taken into account. In our model, the coefficient of light attenuation by water are

constants ($\mathrm{k_{red}}$ k_{red} = 0.225 m^{-1} and $\mathrm{k_{blue/green}}$ $k_{blue/green}$ = 0.0232 m^{-1}, (Manizza et al., 2005), so $z_{iso,tw}$ depends only on the ocean surface irradiance.

Δz_{chl} is the chlorophyll shading effect. It is calculated as the difference between the modeled depth of the isolume and its depth in transparent water ($\Delta z_{chl} = z_{iso} - z_{iso,tw}$). Δz_{chl} quantifies the reduction in isolume depth due to light absorption by chlorophyll.

Δz_{circ} is the ocean circulation effect. It is calculated as the difference between the migration depth of zooplankton and its isolume depth at zenith, i.e. when the isolume is the deepest ($\Delta z_{circ} = z_{mig} - z_{iso}$). Δz_{circ} quantifies variations in migration depth caused by vertical physical transport (advection and mixing), which can move zooplankton away from their isolume faster than zooplankton can respond by swimming.
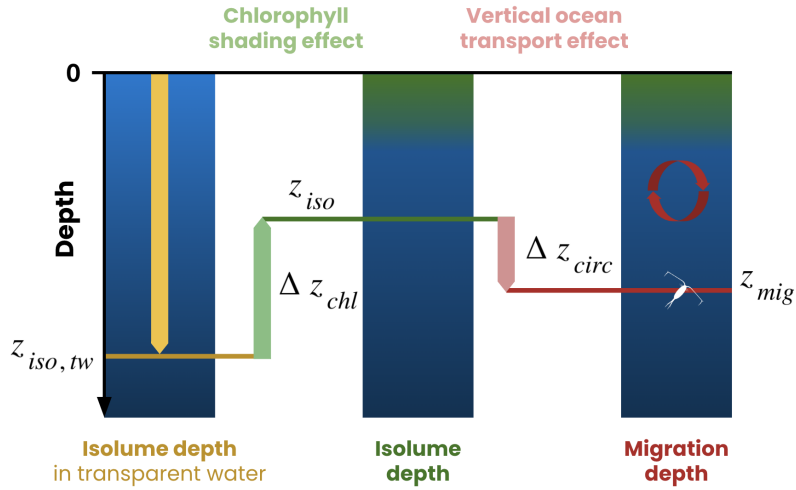
Figure 4. Framework used to identify the processes controlling zooplankton migration depth. The migration depth (z_{mig}, red line) is the sum of the isolume depth in transparent water ($z_{iso,tw}$, yellow line), the chlorophyll shading effect (Δz_{chl}, green arrow) and the vertical ocean transport effect (Δz_{circ}, pink arrow). z_{iso} is the isolume depth targeted by migrating zooplankton. See Methods (Sect. 2.4) for details.

2.4.2 Separation of spatial scales

The chlorophyll content and vertical transport, which control migration depth, respond to large-scale dynamics (>100 km) but are also modulated by fine-scale dynamics (<100 km) such as mesoscale eddies or submesoscale fronts. To isolate these two scales of variability, we perform a spatial Reynolds decomposition. We spatially filter Δz_{chl} and Δz_{circ} using a Gaussian kernel with a standard deviation of 100 km, and write them as the sum of a large-scale average ($\langle \Delta z_{chl} \rangle, \langle \Delta z_{circ} \rangle$) and a fine-scale anomaly (z'_{chl}, z'_{circ}) relative to this average:

$$\Delta z_{chl} = \langle \Delta z_{chl} \rangle + \Delta z'_{chl} \tag{13}$$

$$\Delta z_{circ} = \langle \Delta z_{circ} \rangle + \Delta z'_{circ} \tag{14}$$

In contrast, the isolume depth in transparent water ($z_{iso,tw}$), which depends on surface irradiance, does not vary on fine spatial scales in our simulation because the irradiance forcing is zonally uniform. Consequently, the fine-scale term is almost zero:

$$z_{iso,tw} = \langle z_{iso,tw} \rangle + z'_{iso,tw} \approx \langle z_{iso,tw} \rangle \tag{15}$$

To summarize, this framework provides a way to disentangle the complexity of the mechanisms modulating the migration depth:

$$z_{mig} = z_{iso,tw} + \langle \Delta z_{chl} \rangle + \Delta z'_{chl} + \langle \Delta z_{circ} \rangle + \Delta z'_{circ} \tag{16}$$

We isolate irradiance contribution and distinguish the spatial contributions of chlorophyll shading and vertical transport at large and fine scales. This framework does not include the limitation of migration depth by oxygen, as its concentration is high and does not limit vertical migration in our simulation.

3 Results

3.1 North Atlantic ~~migrating zooplankton~~ biophysical dynamics

~~The~~

3.1.1 Contrasted biogeochemical biomes

The double gyre model reproduces the characteristic physical and biogeochemical dynamics of four biomes of the North Atlantic: a low-productivity subtropical gyre, a high-productivity subpolar gyre, an energetic jet in between with intense mesoscale eddy activity, and a deep winter convection region in the northern part of the domain (Fig. 1, Fig. 5 and Fig. A2). The subtropical, subpolar and jet biomes are defined by thresholds of annual surface chlorophyll concentration (0.15 and 0.35 mg m^{-3}), as used in previous studies (Resplandy et al., 2012, 2019). The convecting region is identified as a subregion of the subpolar region, using the 200-meter threshold on the annual mean mixed layer depth. Our main conclusions are not sensitive to these thresholds. Note that the wind creates an upwelling along the wall at the southern boundary and stimulates ocean productivity with annual mean chlorophyll concentrations higher than 0.35 mg m^{-3} (Fig. 5d). This upwelling, representative of the equatorial dynamics occurring further south in nature, is excluded from the analysis using the chlorophyll thresholds given above.

The mean biophysical conditions and seasonal cycle simulated within the biomes are similar to those observed in the ocean. In both observations and model, the subtropical anticyclonic gyre (elevated sea surface height, Fig. 1a) is oligotrophic at
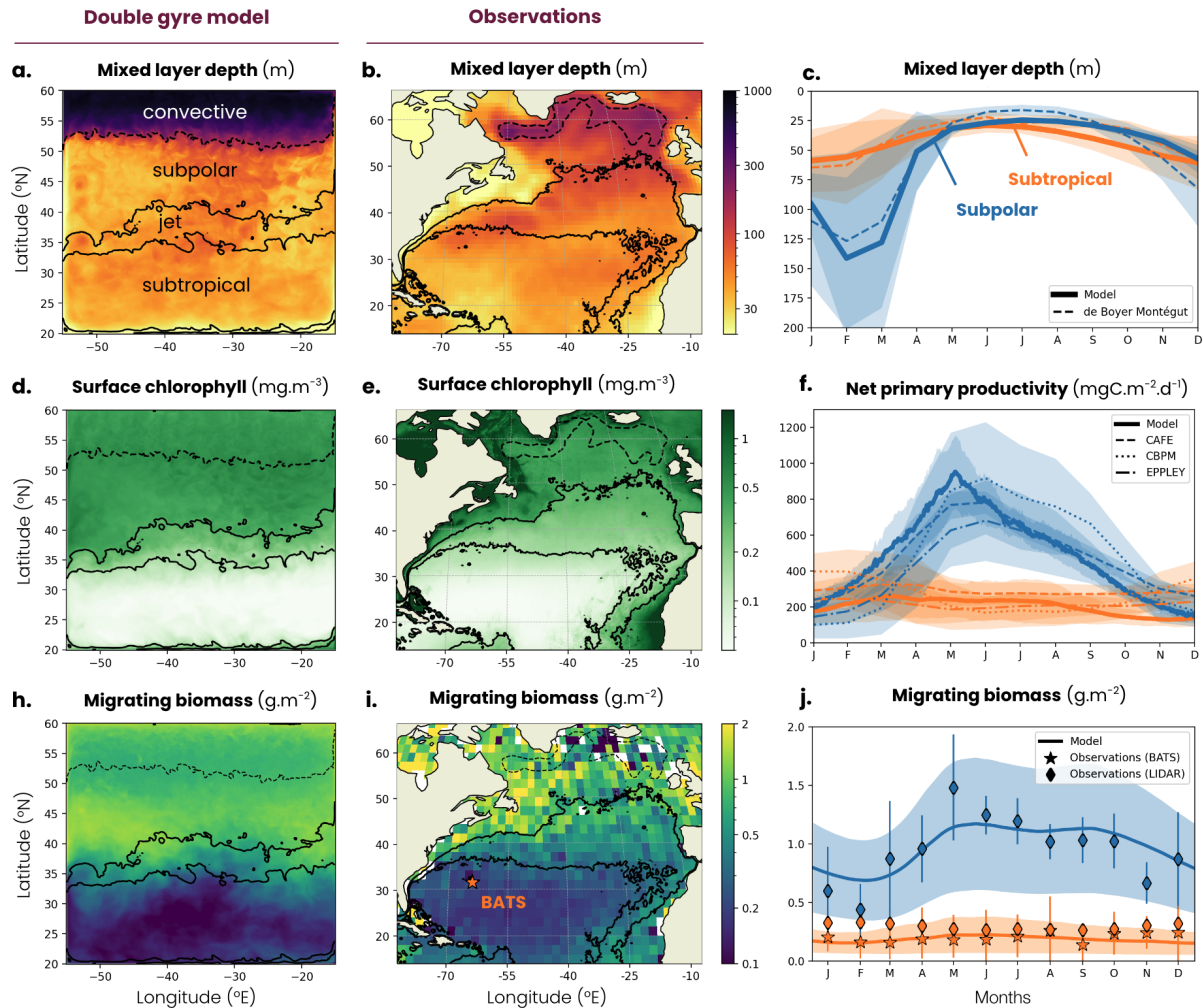
Figure 5. Map of annual mean (a,b) mixed layer depth (MLD), (d,e) surface chlorophyll concentration and (h,i) migrating zooplankton biomass in (a,d,h) the double gyre model and (b,e,i) observation-based data products. The subtropical, jet and subpolar biomes are delimited by solid black lines (mean surface chlorophyll concentration = 0.15 and 0.35 mg m^{-3}), while the subpolar and convective biomes are delimited by a dashed line (mean MLD = 200 m, see Methods). Mean seasonal cycle of (c) MLD, (f) net primary productivity and (j) migrating zooplankton biomass in the subtropical biome (orange) and the subpolar biome (blue) in the the double gyre model (solid lines) and observation-based products (dashed lines). Shading and error bars correspond to two standard deviations around the average. Orange star in (i) indicates the Bermuda Atlantic Time-series Study (BATS). See Sect. 2.2 for observational product details.

the surface, with nitrogen concentrations averaging 0.29 and 0.28 μmolN kg^{-1} respectively, and phosphorus concentrations averaging 0.03 and 0.06 μmolP kg^{-1} in the first 100 meters (Fig. A2a-d). The model also reproduces the observed stratification throughout the year, with a mixed layer varying between 30 and 60 m seasonally (Fig. 5a-c), strongly limiting the supply of

nutrients to the surface. Consequently, net primary productivity in the subtropical gyre is low (between 170 and 250 mgC m^{-2} d^{-1} on average in model and observation-based estimates) and varies little seasonally (Fig. 5d-f). In contrast, the subpolar cyclonic gyre (depressed sea surface height) is a nutrient-rich environment. Nitrate concentrations range from 8 to 17 μmolN kg^{-1} in the top 100 meters, and phosphate concentrations from 0.3 to 0.8 μmolP kg^{-1} (Fig. 1a, Fig. A2a-d) in both observations and model. This is partly due to high seasonality, with a modeled mixed layer averaging 140 m in winter (125 m in observations, Fig. 5c), bringing nutrients to the surface. Consequently, net primary productivity in the subpolar gyre is high and seasonally marked (Fig. 5f). It increases from January onwards, peaks in May (920 mgC m^{-2} d^{-1} in model, 650-930 mgC m^{-2} d^{-1} in observations) and falls back below 500 mgC m^{-2} d^{-1} at the end of summer.

Finally, at the northern boundary, the wind creates a downwelling and a deep convecting water column characterized by winter mixed layers exceeding 1000 meters (Fig. 5a). These deep convection events can be considered as representative of ocean dynamics occurring further north in the Atlantic Ocean, such as the Irminger and the Labrador Seas (Fig. 5b). These convection events bring a high concentration of nutrients to the surface ($>$12 μmolN kg^{-1} and $>$ 0.7 μmolP kg^{-1}, Fig. 1a, Fig. A2a-d) and sustain a biome productivity of 420 mgC m^{-2} d^{-1} on annual average, reaching up to 1250 mgC m^{-2} d^{-1} in spring.

These large-scale dynamics are locally modulated by fine-scale structures such as eddies and fronts (Fig. 1b-e). The jet hosts the most energetic fine-scale dynamics (Fig. 1d, Fig. A3), because it is unstable and therefore induces eddy formation. Many eddies are present in the subtropical gyre, since the horizontal resolution of the model is sufficient to resolve mesoscale dynamics ($>$100 km). Conversely, in the subpolar gyre, the resolution is not sufficient to fully resolve these eddies, leading to less coherent and more filamentary turbulent structures. As we will show in this study, these features introduce variability in the gyre and seasonal dynamics and are key to understand zooplankton migration depth variability.

3.1.2 North Atlantic migrating zooplankton dynamics

The model reproduces the regional and latitudinal contrasts in biomass and fraction of migrating zooplankton observed in the North Atlantic (Fig. 5h-j, Fig. A5). In the subpolar biome, the migrating zooplankton biomass and seasonal variations are high in both the model and LIDAR estimates (1 $\pm$ 0.5 g m^{-2}, Fig. 5c), reflecting the high productivity and seasonality of this biome (Fig. 5d-f). Migrating biomass is minimal in late winter (0.69 $\pm$ 0.34 g m^{-2}), accumulates in spring and peaks in May (1.17 $\pm$ 0.57 g m^{-2}). Biomass remains high throughout summer and fall (1.11 $\pm$ 0.54 g m^{-2}), before declining in November. In contrast, the subtropical biome is characterized by lower biomass and low seasonality in both model and observations (0.18 $\pm$ 0.12 g m^{-2}, Fig. 5h-j), reflecting the low productivity and seasonality of the region (Fig. 5d-f). Migrating zooplankton account for about half of the medium- and large-sized zooplankton in the model in both biomes, which is in line with observations from the COPEPOD database ~~compiled by (Aumont et al., 2018, Fig. A5)~~(Aumont et al., 2018, Fig. A5).

The model also reproduces the timing of zooplankton migration. The ADCP observations compiled by Bianchi and Mislan (2016) show a linear relationship between the length of the day and the time spent at depth by migrating zooplankton (Fig. 2b). The longer the days, the longer migrating zooplankton remain at depth. This relationship is reproduced in the model. Migrating zooplankton spend between 9 and 18 hours at depth depending on the length of the day. Since the day length is less variable
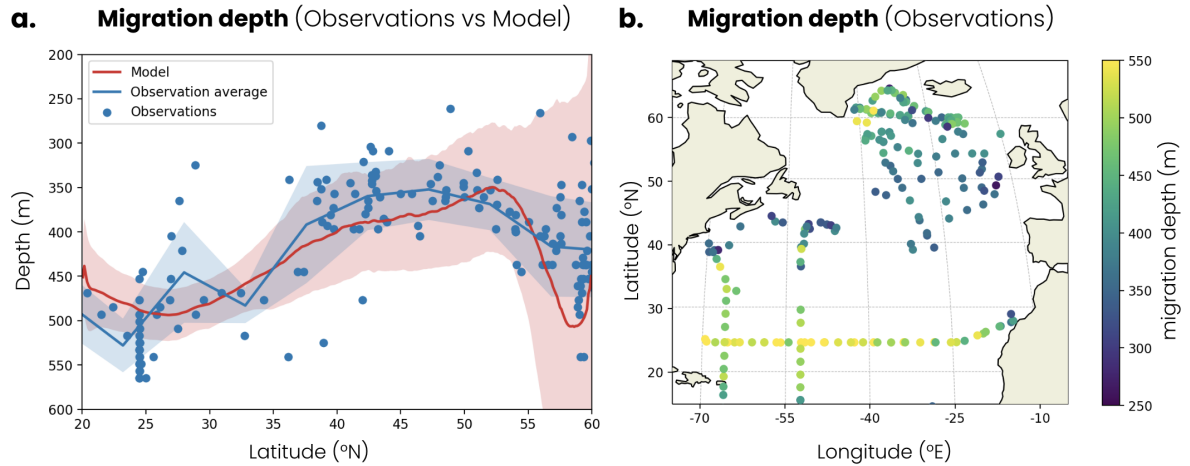
Figure 6. (a) Latitudinal distribution of migration depth. Blue dots are observations derived from acoustic doppler current profiler (ADCP) observations and the blue line their average per 5° latitude bins. Red line is the zonal and temporal average of the model. The shading corresponds to two standard deviations around the average. (b) Migration depth derived from ADCP observation in the North Atlantic used in panel a.

over the year at low latitudes than at high latitudes, the same applies to the time spent at depth by migrating zooplankton. In the subpolar biome, migrating zooplankton stay at depth on average 10 hours in winter and 18 hours in summer, while in the subtropical biome, ~~it stays~~ they stay at depth on average 11 hours in winter and 15 hours in summer.

Finally, the model reproduces the contrasts in migration depths observed in the North Atlantic. Zooplankton migration depths vary both across and within biomes. ADCP observations show that zooplankton dive about 100 m deeper in the subtropical biome, where the average migration depth is 480 m, than in the subpolar biome, where it is confined to 370 m (Fig. 6a,b). The model reproduces these large-scale contrasts with an average migration depth of 480 m in the subtropical biome and 380 m in the subpolar biome (Fig. 6a). The jet region, around 40° N, shows intermediate migration depths of around 340 m in both observations and our model. Observations also show migration depth variability within biomes, up to 100 to 200 meters around the biome average, which is relatively well captured by the model (shading on Fig. 6a). The model simulates migration depth and variability in the convective biome that are higher than observed at 55-60° N. The simulated mean migration depth is over 450 m, whereas observations show depths of around 420 m, and variability in the model is three times greater than in observations. However, these deep convection events occur further north in nature, as in the Irminger Sea, where migrations have been observed below 500 m (Fig. 6b). Furthermore, in these deep convection regions, some zooplankton replace their daily migratory behaviour with seasonal migratory behaviour for part of the year (see discussion Sect. 4).

3.2 Controls of zooplankton migration depth

The observed migration depth and its variability result from the combination of processes varying on different space and time scales, which cannot be disentangled from the limited number of observations available. In the following, we therefore use the model, which reproduces the observed patterns, to investigate the mechanisms controlling the large spatial contrast between the subtropical and subpolar gyres, the variability introduced at fine-scales ($>$100 km) by eddies and filaments, as well as the influence of seasonality. We identify chlorophyll shading as a major mechanism in regulating migration depth, although the contribution of ocean transport in the convective region and the seasonality of surface irradiance are significant. Only results for medium migrating zooplankton are presented. Results for large migrating zooplankton are similar, but where differences arise, they are indicated as such and presented in supplementary materials (Fig. B1, B2).

3.2.1 Mechanisms modulating zooplankton migration depth

Zooplankton migration depth is modulated by three mechanisms: surface irradiance, chlorophyll shading and ocean vertical transport (see Methods, Sect. 2.4). We illustrate the influence of these three effects using model snapshots and a depth-latitude section across the different biomes early in the ~~Spring~~ spring bloom (March 1st, Fig. 7). First, migrating zooplankton target a specific isolume whose depth depends on surface irradiance intensity. As surface irradiance increases, light penetrates further into the water column, resulting in a deeper isolume. We track the isolume depth as if the water were transparent ($z_{iso,tw}$) to isolate this irradiance effect. For example, Figure 7 shows that on March 1st, $z_{iso,tw}$ is slightly deeper in the subtropical gyre than in the subpolar gyre, because surface irradiance at zenith is stronger at low latitude than at high latitude (yellow line and arrow on Fig. 7d).

Seawater contains chlorophyll, which modifies light penetration in the water column by changing its opacity. As chlorophyll content increases, water opacity and chlorophyll shading increase resulting in a shallower isolume (z_{iso}, Fig. 7, green line ~~on~~ in panel d). Shallow migration regions are characterized by high chlorophyll content and deep migration regions by low chlorophyll content. This chlorophyll shading effect (Δz_{chl}, green arrow), acts on large scale, between the subtropical and subpolar biomes, but also at the scale of eddies and filaments, where migration depths can vary by up to 200 m between points that are only 20 km apart with chlorophyll content that differ by more than 60 mg m^{-2} (Fig. 7a,b).

Finally, migrating zooplankton can be transported away from their isolume when ocean vertical transport associated with advection and/or turbulent mixing is high. For example in the convective biome, vertical ocean transport (Δz_{circ}, red arrow) carries migrating zooplankton more than 200 m below their isolume (Fig. 7d). This occurs during deep convection events where the mixed layer exceeds 1000 m (Fig. 7c).

3.2.2 Controls of migration depth spatial variability at large-scale

We generalize our analysis by evaluating the average annual effect of irradiance, chlorophyll shading and vertical transport on migration depth across the four biomes (Fig. 8). We find that the spatial contrast in migration depth between the different biomes is mainly due to differences in chlorophyll shading. On annual average, the effect of irradiance ($z_{iso,tw}$) is similar across
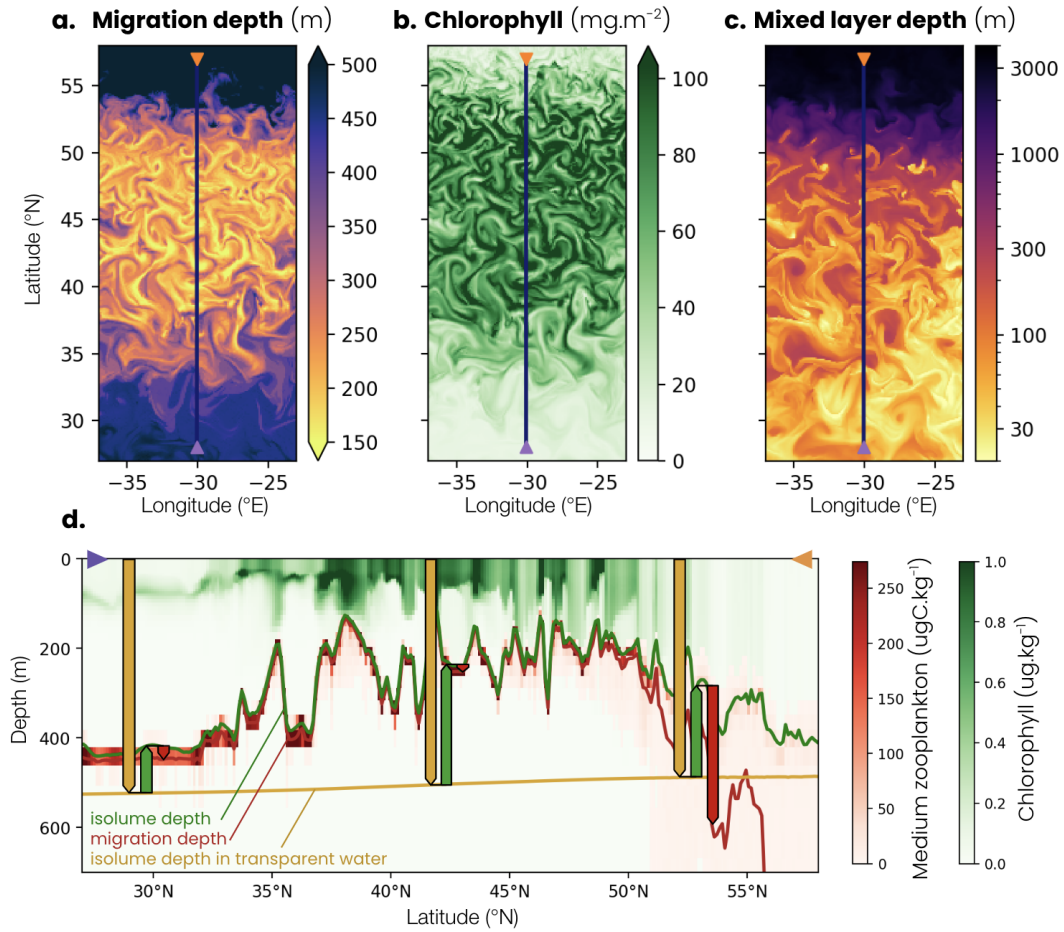
Figure 7. Snapshot on March 1st 1st of (a) biomass-weighted medium zooplankton migration depth at zenith, (b) water column chrophyll content and (c) mixed layer depth. The blue line corresponds to the location of the cross-section shown on panel d. (d) Vertical cross-section of chlorophyll (green) and medium zooplankton (red) concentration on March 1st 1st, at 30° E, between 27° N and 57° N. The depth-latitude section also shows transparent-water isolume depth (yellow line), isolume depth (green line) and migration depth (red line) at zenith. The transparent water isolume depth is a baseline controlled by irradiance intensity (yellow arrows), the difference between isolume and transparent water isolume depths is caused by chlorophyll shading (green arrows) and the difference between migration depth and isolume depth is the effect of ocean vertical transport (red arrows).

the four biomes (yellow bars in Fig. 8). Without other factors, irradiance in transparent waters would lead to migration down to 480 m in the subtropical biomes where irradiance is highest, and down to 440 m in the convective biome where irradiance is lowest.

Large-scale chlorophyll shading ($\langle \Delta z_{chl} \rangle$) reinforces the weak latitudinal contrast set by irradiance, reducing migration depth by about 100 m on annual average in the less productive subtropical gyre, while it reduces it by approximately 140-165
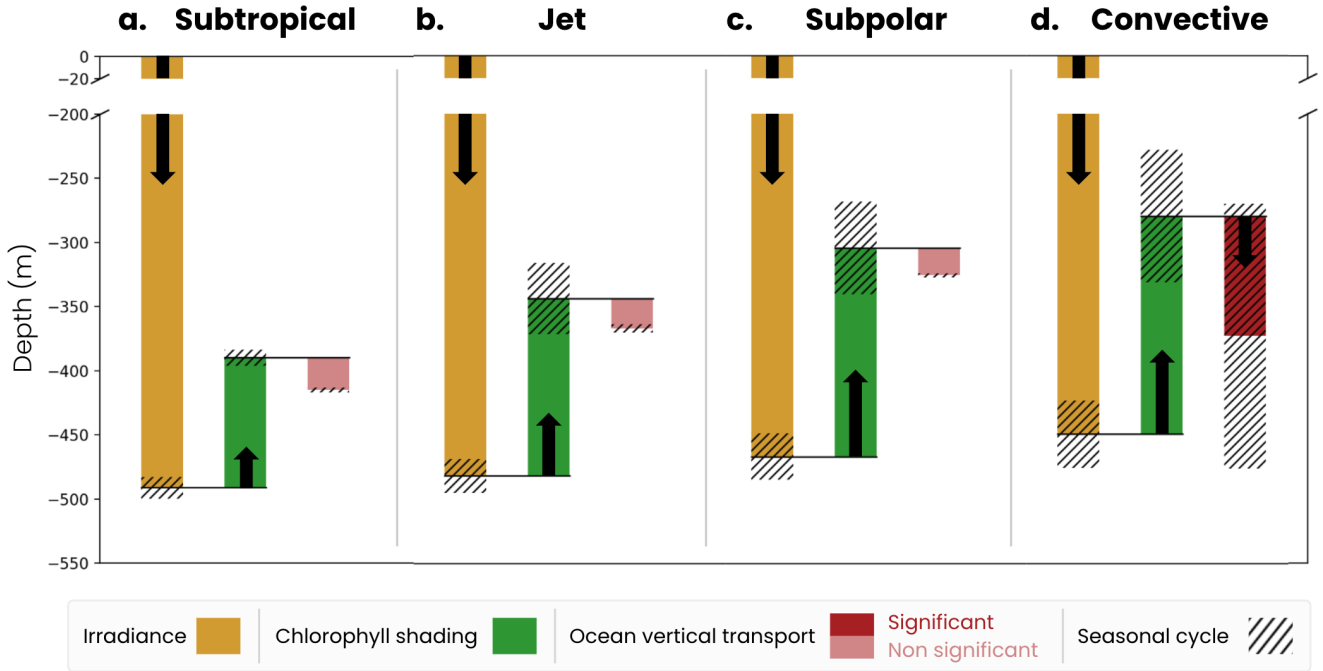
Figure 8. Mechanisms controlling the migration depth of medium zooplankton on annual average in the (a) subtropical, (b) jet, (c) subpolar and (d) convective biomes. The decomposition includes the effects of large-scale variations in irradiance ($z_{iso,tw}$, yellow bar), chlorophyll shading ($\langle \Delta z_{chl} \rangle$, green bar) and vertical ocean transport ($\langle \Delta z_{circ} \rangle$, red bar), and their seasonal range of variability (black hatch). The effect of transport is non-significant (light red bar) when it is smaller than the vertical resolution of the model grid at that depth.

m in the more productive jet region and subpolar gyre, and by up to 180 m in the convective region (Fig. 8a-c, dark green bars, see in Fig. 5d-f for annual mean chlorophyll). In the convective biome, the effect of ocean vertical transport ($\langle \Delta z_{circ} \rangle$) partially offsets that of chlorophyll shading. Migrating zooplankton are transported 100 m below their isolume on annual average due to deep convection events. In other regions, the effect of transport is not significant ($\langle \Delta z_{circ} \rangle$ lower than the model vertical grid resolution at the depth of migration, Fig. 8a-c). The migration depth of large zooplankton is 100 m deeper than that of medium zooplankton due to irradiance, since they follow a darker isolume. However, the modulation of their migration depth by chlorophyll shading and transport is similar to medium zooplankton (Fig. B1). We note that the chlorophyll shading effect is not sensitive to the choice of parameters in the migration model (e.g., target isolume, migration velocity, Fig. B3).

3.2.3 Controls of migration depth seasonal variability

Migration depth is modulated on the seasonal time-scale in response to variations in irradiance, bloom dynamics (i.e., chlorophyll absorption) and winter convection (Fig. 9). Seasonal irradiance variations deepen the migration depth in summer (deep $z_{iso,tw}$) and decrease it in winter (shallow $z_{iso,tw}$) compared to its average annual effect (Fig. 9, yellow line). The ampli-

455   tude of seasonal variations in the irradiance effect increases with latitude (subtropical: 25 m, jet: ~~40m~~ 40 m , subpolar: 57 m,
convective: 85 m) due to greater variations in the solar incidence angle.

     Large-scale chlorophyll shading considerably reduces migration depth during the spring phytoplankton bloom when chloro-
phyll content is highest (Fig. 9, green line). In productive regions, this reduction in the migration depth is most pronounced
between February and May, and intensifies with latitude due to a more pronounced and prolonged phytoplankton bloom. The

460   seasonal reduction in migration depth attributable to chlorophyll shading reaches 190 m in the jet region, 235 m in the subpolar
gyre, and 300 m in the convective region (Fig. 9b-d). In contrast, there ~~is~~ are no seasonal variations in the chlorophyll shading
in the subtropical gyre (Fig. 9a). Large-scale vertical transport deepens the migration depth in the convective region during
convective events between January and April, down to -340 m at its peak (Fig. 9, red line). This effect is negligible at other
times and in other regions.
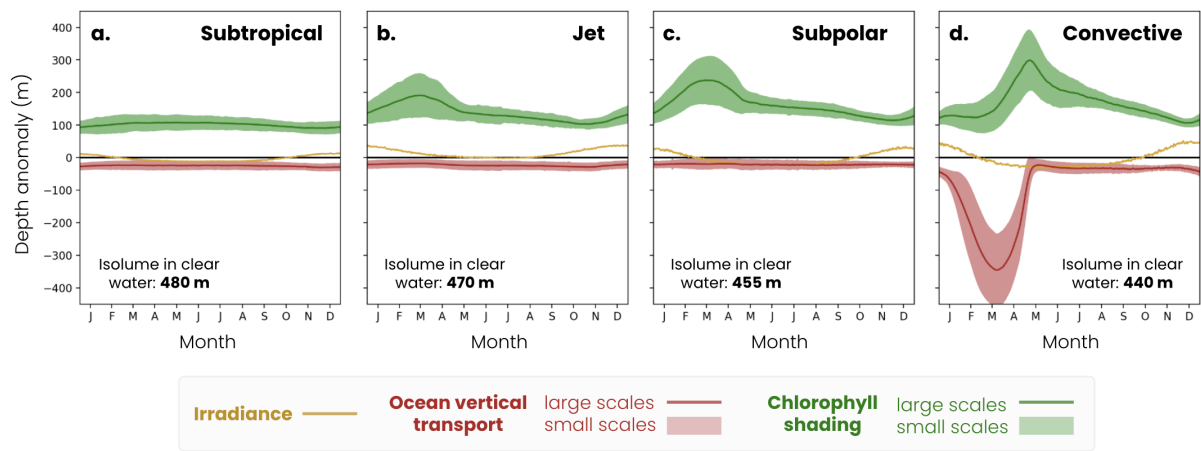
Figure 9. Mechanisms controlling the medium zooplankton migration depth seasonal (solid lines) and fine-scale (<100 km, shading enve-
lope) variability in the (a) subtropical biome, (b) jet, (c) subpolar and (d) convective biomes for the irradiance ($z_{iso,tw}$ in yellow), chlorophyll
shading ($\langle\Delta z_{chl}\rangle$ and $\Delta z'_{chl}$ in green) and vertical transport ($\langle\Delta z_{circ}\rangle$ and $\Delta z'_{circ}$ in red) effects. Contributions are relative to the baseline
depth set by mean annual irradiance (isolume in transparent water, decreasing from 520 m in the subpolar gyre to 480 m in the convective
region, see in Figure 8).

465   **3.2.4   Controls of migration depth spatial variability at fine-scales**

    Within biomes, patchiness in phytoplankton and mixed layer depths introduces strong variations in the chlorophyll shading
and transport effects ($\Delta z'_{chl}$ and $\Delta z'_{circ}$), and modulate the migration depth at fine spatial scales as shown by the snapshots
from March ~~1st~~ 1st (Fig. 7a-c). The amplitude of this fine-scale variability depends on the biome and the time of year, with
stronger fine-scale variability found in late winter and spring in the jet, subpolar and convective biomes (Fig. 9). On average,

470   the chlorophyll fine-scale effects have a larger impact on migration depth than the fine-scale effects of transport. The only
exception is in the convective region, where chlorophyll and transport fine-scale effects are similar.

During the spring bloom, fine-scale variations in chlorophyll and the associated shading (Fig. 9, green filling) modulate the migration depth by $\pm$ 67 m in the jet, $\pm$ 75 m in the subpolar gyre and $\pm$ 100 m in the convective region (Fig. 9b-d, green shading) and are smaller during the rest of the year (less than $\pm$ 30 m). In other words, this fine-scale effect can create migration

475 depth contrasts of up to 200 meters between two spots 10-20 km apart during spring bloom in productive regions, reinforcing or offsetting the large-scale chlorophyll shading effect. This fine-scale chlorophyll shading effect is however much weaker ($\pm$ 20 m) and shows little seasonal variations in the subtropical gyre waters containing less chlorophyll (Fig. 9a).

In the convective region, the fine-scale effect of transport (Fig. 9, red filling) is high from January to April, and modulates migration depths up to $\pm$ 135 m, due to local changes in the mixed layer depth (Fig. 7c). During the rest of the year and in other

480 regions, the fine-scale ocean transport effect is not significant. Thus, although these fine-scale effects are small on an annual average (less than $\pm$ 40 m), they can significantly modulate the migration depth from late winter to spring.

4 Conclusions and Discussions

In this study, we have developed a mechanistic zooplankton vertical migration model, which we integrated into a large-scale ocean biogeochemical model and implemented in an idealized, high-resolution double gyre physical framework. This model

485 reproduces the large-scale contrasts in zooplankton migration depth observed between the North Atlantic subtropical and subpolar biomes (480 m vs. 380 m) (Bianchi et al., 2013b). It also captures seasonal variations similar to those observed by Hobbs et al. (2021), with a migration depth decreasing by around a hundred meters during the phytoplankton bloom. Furthermore, the model depicts variations in migration depth on fine spatial scales (<100 km) consistent with those observed across a front by Powell and Ohman (2015), with migration depths varying by up to 200 m between points 10-20 km apart.

490 In the model, these large-scale, fine-scale and seasonal variations in migration depth are largely caused by the shading of chlorophyll contained in the water column, decreasing the depth of the isolume targeted by migrating zooplankton. Chlorophyll shading leads to differences in migration depth of about 60 meters m on annual average between the subtropical biome (low productivity / low chlorophyll shading) and the subpolar biome (high productivity / high chlorophyll shading), and up to 150 meters m during the spring bloom. In contrast, variations in migration depth caused by differences in surface irradiance between

495 biomes are relatively small (<40 m), although we note that seasonal variations within biomes are significant (60 to 85 meters m in the subpolar and convective biomes). We find that large-scale difference in chlorophyll shading effect across biomes can be reinforced or offset by 100 meters m locally by fine-scale ocean dynamics associated with eddies, fronts that lead to patchy chlorophyll distribution (Gaube et al., 2014). This patchiness in chlorophyll is consistent with prior studies that showed fine-scale dynamics could create strong horizontal gradients in chlorophyll content through horizontal stirring (e.g., Martin,

500 2003), or through the stimulation of phytoplankton growth by local vertical supply of nutrients and changes in light exposure (e.g., Lévy et al., 2018). Also, contrasts in migration depth caused by differences in surface irradiance between biomes are relatively small (<40 m) but seasonal variations within biomes are significant, ranging from 60 to 85 meters m in the subpolar and convective biomes.

These results suggest that the ability of migrating zooplankton to sequester carbon in the interior ocean could be limited by chlorophyll shading on both ~~large-scale~~ the large- and fine-scale. Productive chlorophyll-rich regions, such as the subpolar gyre at large scale or phytoplankton-rich filaments at ~~fine scale~~fine-scale, provide abundant food for zooplankton and are the regions where migrating zooplankton export the most carbon (Lévy et al., 2018; Mangolte et al., 2023; Kaiser et al., 2021; Aumont et al., 2018; Archibald et al., 2019; Nowicki et al., 2022). However, it is also in these regions that chlorophyll shading reduces migration depth the most. The carbon exported by migrating zooplankton in productive regions could therefore be sequestered for a shorter time, as the shallower the migrating zooplankton excrete or respire carbon, the faster it takes for ocean circulation to bring it to the surface, reducing the time it is potentially sequestered in the ocean interior (Boyd et al., 2019).

The model suggests that large-scale ocean transport can further modulate the migration depth, but this effect is confined to deep convective events during which zooplankton can be transported up to 330 m below their isolume. In nature, this process could potentially influence zooplankton migration in the Irminger, Greenland or Labrador Seas, where deep convection events occur (Våge et al., 2009; Piron et al., 2017; Sgubin et al., 2017). Our results also suggest that fine-scale ocean dynamics, restratifying the mixed layer and causing patchiness in ocean transport (Mahadevan, 2016; Resplandy et al., 2019), can lead to migration depth differences up to 250 m between two locations 10-20 kilometers apart in the convective biome. However, these results are probably overestimated for two reasons. First, our idealized wind creates an intense downwelling in the convective biome at the northern boundary of the model, leading to the convection of the entire water column (MLD > 3500 m, Fig. 5a,c, Fig. A4c), while mixed layer depths observed in the Labrador, Irminger and Greenland Seas are around 200-500 m on average and up to 1500-2000 m at most (Holte et al., 2017; Gonzalez-Pola et al., 2020). Second, in nature, part of the zooplankton community stops diel vertical migration to enter into diapause under the permanent thermocline (600-1,400 m) in winter in the North Atlantic (Jónasdóttir et al., 2015), a process not accounted for in our model. At these depths, zooplankton in diapause could be less affected by deep convection. Therefore results in the convective biome should be considered with caution.

Existing biogeochemical models that include zooplankton vertical migration primarily use light to control diel migration patterns (Bianchi et al., 2013b; Aumont et al., 2018; Archibald et al., 2019; Nowicki et al., 2022). In contrast, our model introduces a novel prey-driven redistribution mechanism at night, where zooplankton adjust their vertical positions to optimize feeding opportunities by aligning with depths of higher prey concentration, which more accurately captures the critical role of prey availability in shaping zooplankton behavior (Dini and Carpenter, 1992; Beklioglu et al., 2008). However, the model is limited by the lack of predator-led controls, partly because key zooplankton predators are not explicitly represented. This omission could oversimplify zooplankton migration behavior, especially in regions where predator pressure is significant (Bollens and Frost, 1989). In reality, zooplankton DVM is influenced by a balance between avoiding predators and optimizing feeding, with predator pressure often modulating the depth and timing of migrations (Hays, 2003; Bandara et al., 2021). Future improvements could aim to integrate predator-prey interactions more comprehensively to enhance the realism and applicability of the model across various marine environments (Pinti et al., 2019).

This study highlights the role of chlorophyll in setting the zooplankton migration depth in the North Atlantic. Other studies have underlined the importance of other environmental variables such as moonlight (Last et al., 2016) or ice cover (Petrusevich et al., 2016; Flores et al., 2023) modulating the light landscape and the isolume depth in the Arctic regions, cloud shadow in the

subpolar North Pacific (Omand et al., 2021), or the oxygen concentration limiting zooplankton migration in the upper margin of oxygen minimum zones (Bianchi et al., 2013a). Although estimates are uncertain, climate models predict that most of these parameters will evolve in response to climate change (Kwiatkowski et al., 2020; Notz and Community, 2020; Vignesh et al., 2020).A decrease in ocean productivity or ice cover could deepen the isolume and ocean deoxygenation could alter migration depth in oxygen-limiting regions. Moreover, zooplankton size is one of the main features controlling their migration depth (Ohman and Romagnan, 2016). Warmer and less productive waters tend to support smaller zooplankton communities (Barton et al., 2013; Brun et al., 2016) which could dive to shallower depths. The diversity and complexity of these processes make it difficult to predict the evolution of zooplankton migration depths in the future around the globe. However, COBALTv2-DVM captures all these mechanisms, and its implementation in a global ocean model could provide a way of quantifying their importance.

The patchiness of zooplankton migration depth caused by chlorophyll in spring makes it difficult both to observe migration patterns and their consequences in the ocean. The patchiness of phytoplankton, which has been discussed for a long time (Mackas et al., 1985; Abraham, 1998; Martin et al., 2002), is easily observable from satellites (Lehahn et al., 2018; McClain et al., 2022). However, chlorophyll heterogeneity spreads to the migration depth of zooplankton, which is difficult to measure. Currently, migration depth is mainly derived from ADCP profiles (Bianchi et al., 2013b; Riquelme-Bugueño et al., 2020; Cisewski et al., 2021) or net measurements (Steinberg et al., 2008; Conroy et al., 2020). These observations are expensive because they are carried out from ships during oceanographic campaigns. Consequently, they are too sparse to resolve and isolate signals of large- and fine-scale spatial variability, as well as the seasonal cycle of migration depth in many regions of the ocean (Bianchi et al., 2013a). Yet, migration signatures have already been observed by ARGO floats (Fig. S3 in Boyd et al., 2019). Developing algorithms to detect these migrations in ARGO floats, as has already been done to detect subduction events (Llort et al., 2018) or deep chlorophyll maxima (Cornec et al., 2021), could be incorporated into integrative observational approaches (Bandara et al., 2021) and increase the number of observations available. More observations of zooplankton migration are crucial to better understand its variability, constrain it in ocean models and assess its impact on biogeochemical cycles.

Code availability. The COBALTv2-DVM model and idealized double gyre configuration presented in this paper are available on github at https://github.com/mpoupon/MOM6_Double_Gyre.

Author contributions. Conceptualization: MP, LR, JL. Data curation: MP. Formal analysis: MP. Funding acquisition: LR, JL. Investigation: MP. Methodology: MP, LR, JL. Software: MP, JL, JG, NZ. Supervision: LR, JL, CS. Visualization: MP. Writing – original draft: MP, LR. Writing – review and editing: MP, LR, JL, JG.

Competing interests. The authors declare that they have no conflict of interest.

Acknowledgements. We thank John Dunne for conducting the GFDL internal review. The study has been supported by the National Science
570   Foundation (Eddy effects on Biological Pump award number 2023108).

Appendix A: Materials and Methods
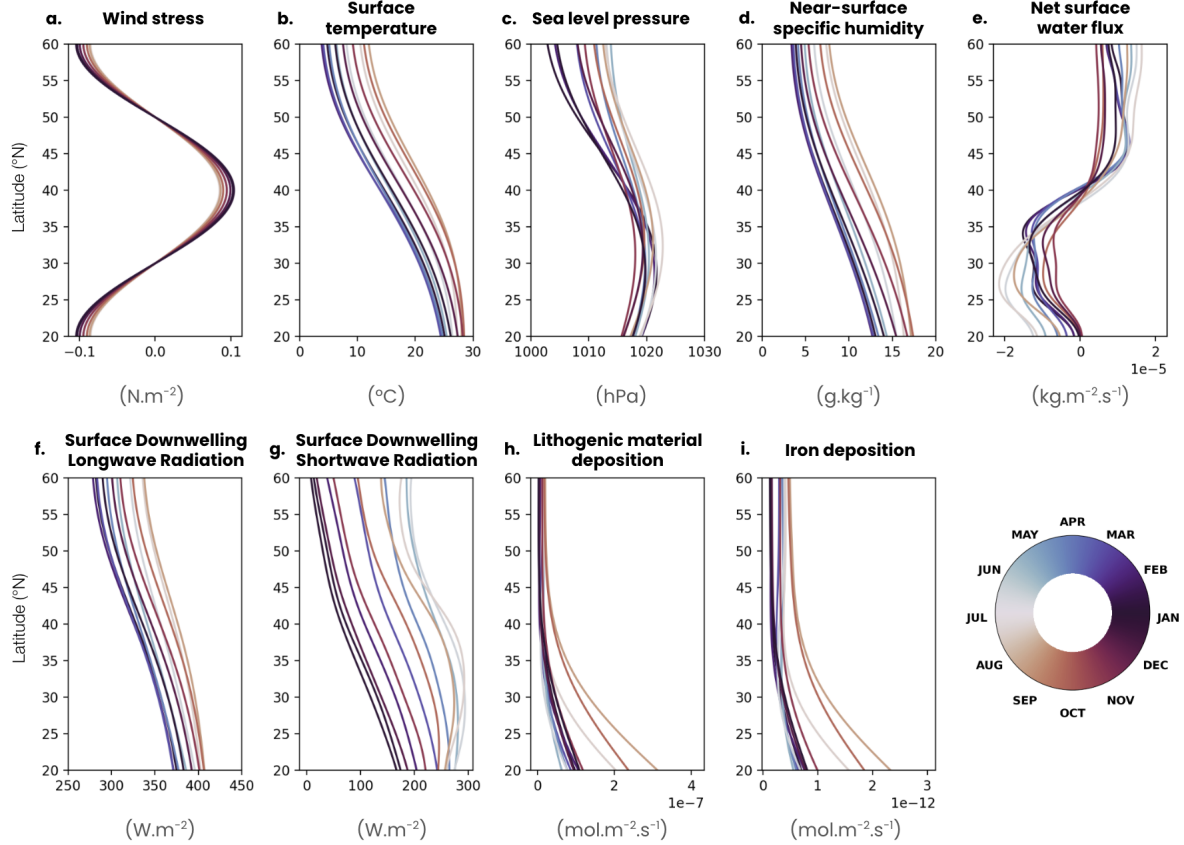
Figure A1. Surface forcing seasonal cycle in the double gyre model. (a) Zonal wind stress following an idealized sinusoidal profile varying by 10% in amplitude according to a seasonal cycle. (b) Atmosphere surface temperature, (b) Sea level pressure, (d) Near-surface specific humidity and (e) precipitation derived from the JRA55-do atmospheric reanalysis (Tsujino et al. 2018), with a 3-h time resolution averaged over the period 1958-2020, and zonally of the North Atlantic Ocean (longitude = -65° E to -20° E, latitude = 20° N to 60° N). Surface downwelling (f) longwave and (g) shortwave radiation calculated as the zonal mean of the the ERA5 atmospheric reanalysis (Hersbach et al. 2020) averaged over the 1979-2022 period and zonally over a band located in the middle of the North Atlantic (longitude = -35° E to -33° E, latitude = 20° N to 60° N). Deposition of (h) lithogenic material and (i) iron deposition are calculated from the last 30 years of a GFDL-ESM4 pre-industrial control simulation spanning from 1850 to 2014 in the same way as the physical forcings (Dunne et al. 2020). Each profile is to the monthly average of the variables and the color corresponds to the month.
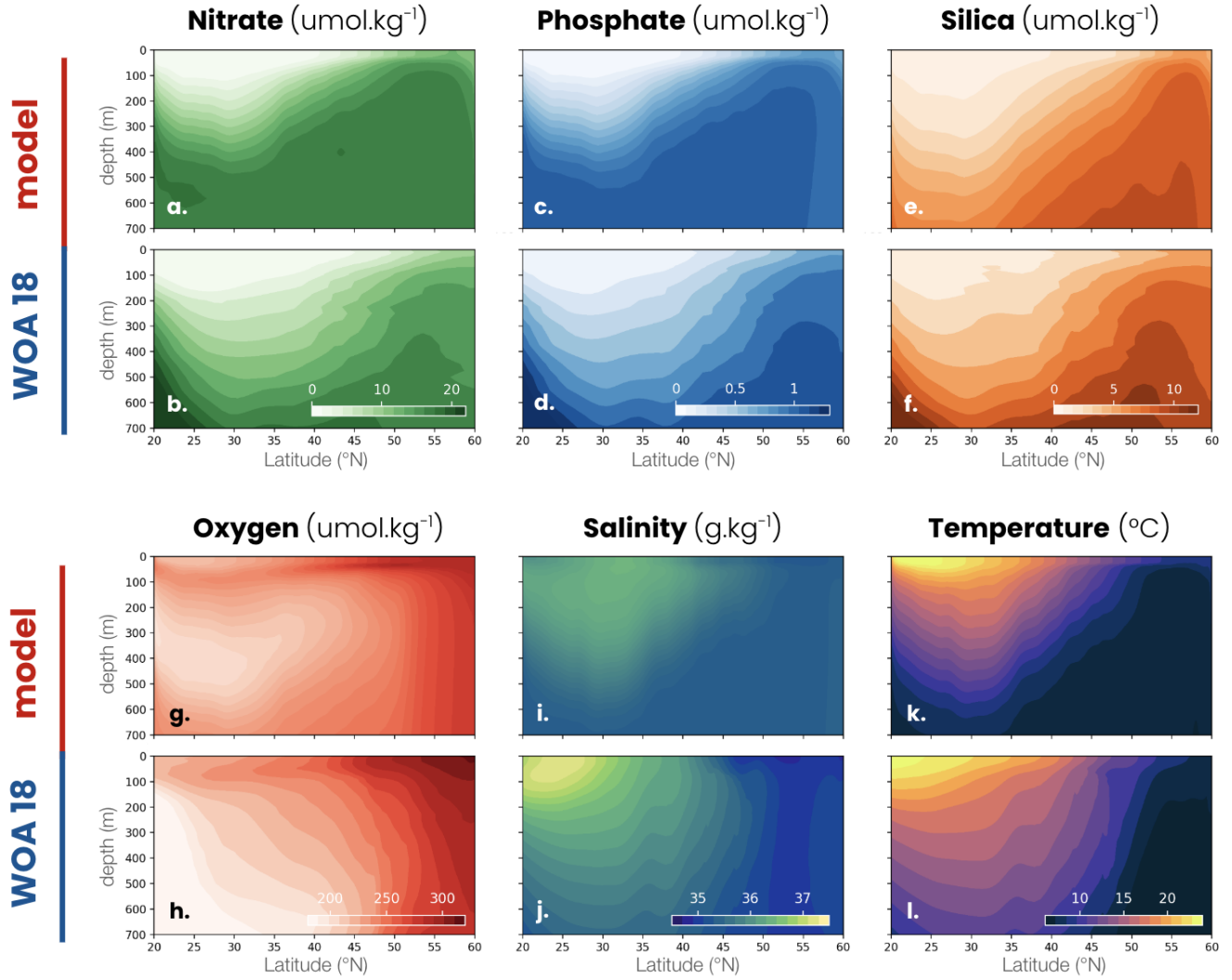
Figure A2. Comparison between the double gyre model and the World Ocean Atlas 2018 (WOA18). Zonal mean of (a,b) nitrate concentration, (c,d) phosphate concentration, (e,f) silica concentration, (g,h) oxygen concentration, (i,j) salinity and (k,l) temperature in the double gyre model (top row) and WOA18 (bottom row, -60° E to -20° E and 20° N to 60° N).
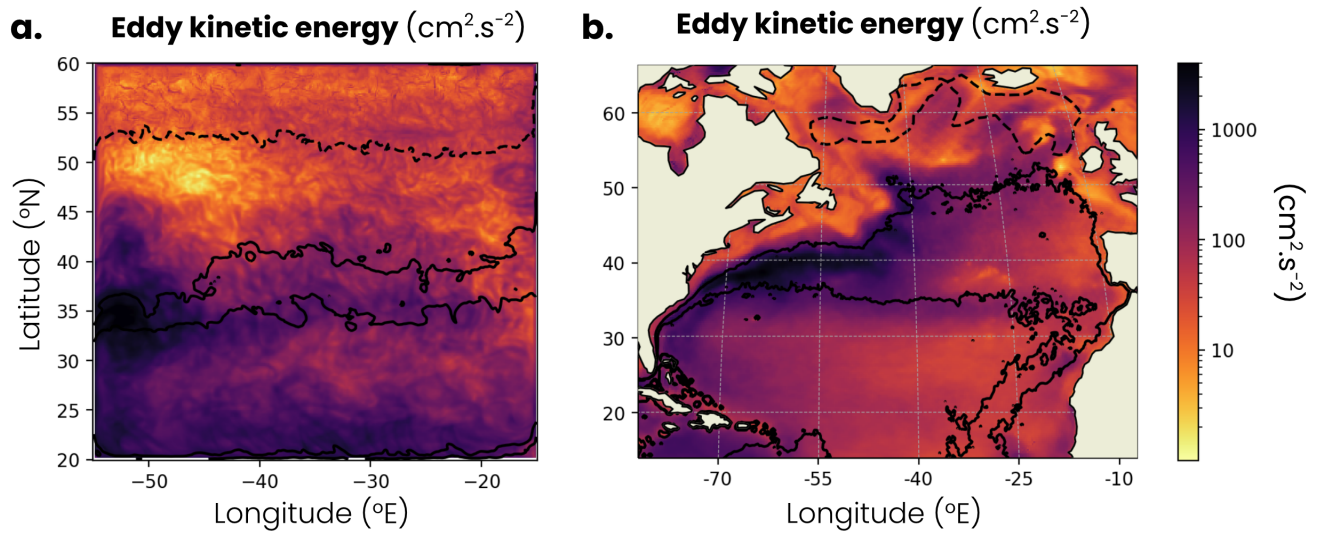
Figure A3. Map of annual mean surface eddy kinetic energy (a) in the double gyre model and (b) derived from sea surface height observations between 1993 and 2021 (Archiving, Validation and Interpretation of Oceanographic Satellite Data - AVISO). The subtropical, jet and subpolar biomes are delimited by solid black lines (mean surface chlorophyll concentration = 0.15 and 0.35 $mg.m^{-3}$), while the subpolar and convective biomes are delimited by a dashed line (mean MLD = 200 m).
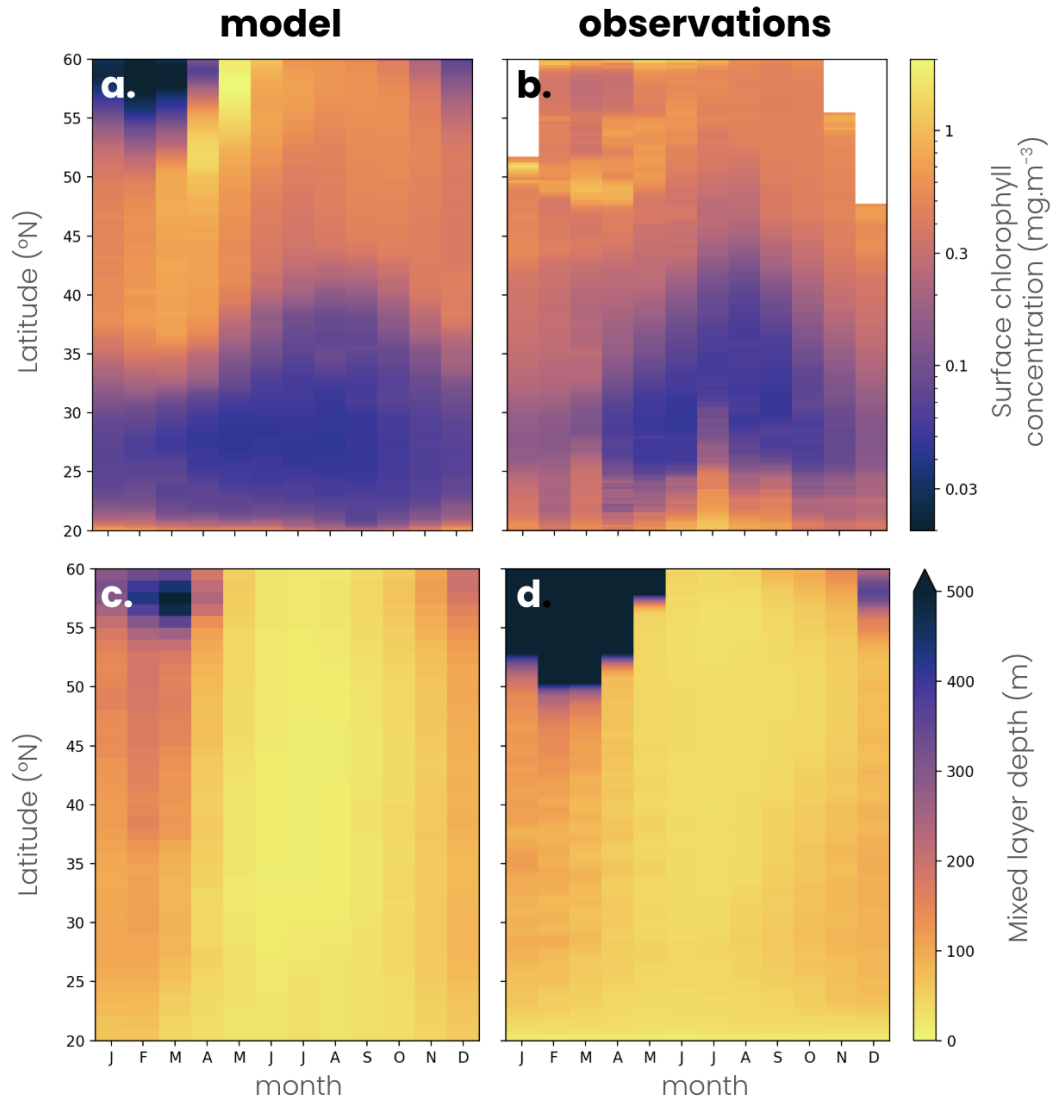
Figure A4. Seasonal cycle of (a,b) surface chlorophyll concentration and (c,d) mixed layer depth in (a,c) the double gyre model and (b,d) observations as a function of latitude. The seasonal cycle is calculated as the zonal mean over the whole domain in the model and in a North Atlantic box (longitude = -65° E to -20° E, latitude = 20° N to 60° N) in the observations. Observations of mixed layer depths are derived from a compilation of hydrographic sections between 1941 and 2002 (de Boyer Montegut et al. 2004), and surface chlorophyll from satellite observations between 1997 and 2020 (Sathyendranath et al. 2019).
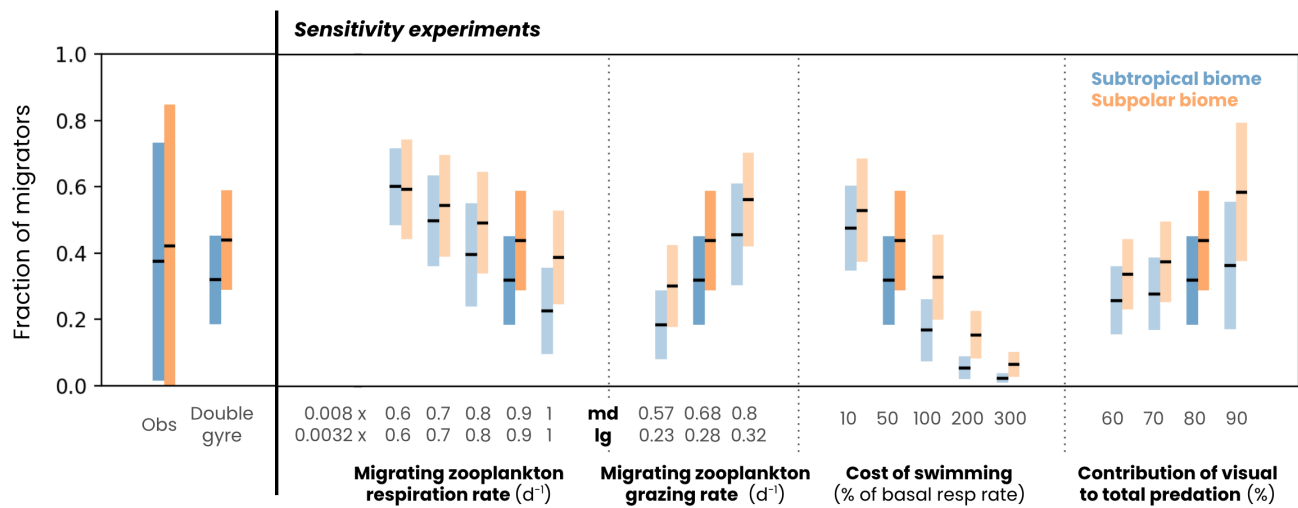
Figure A5. Fraction of zooplankton migrating in the subtropical (blue) and subpolar (orange) biomes in observations (from the COPEPOD database and compiled by Aumont et al. 2018), the double gyre model and a series of sensitivity experiments. The black line corresponds to the mean and the bars to two standard deviations around the mean. The dark blue and orange bars correspond to the simulation described in the paper and the light blue and orange bars to the parameter sensitivity experiments.
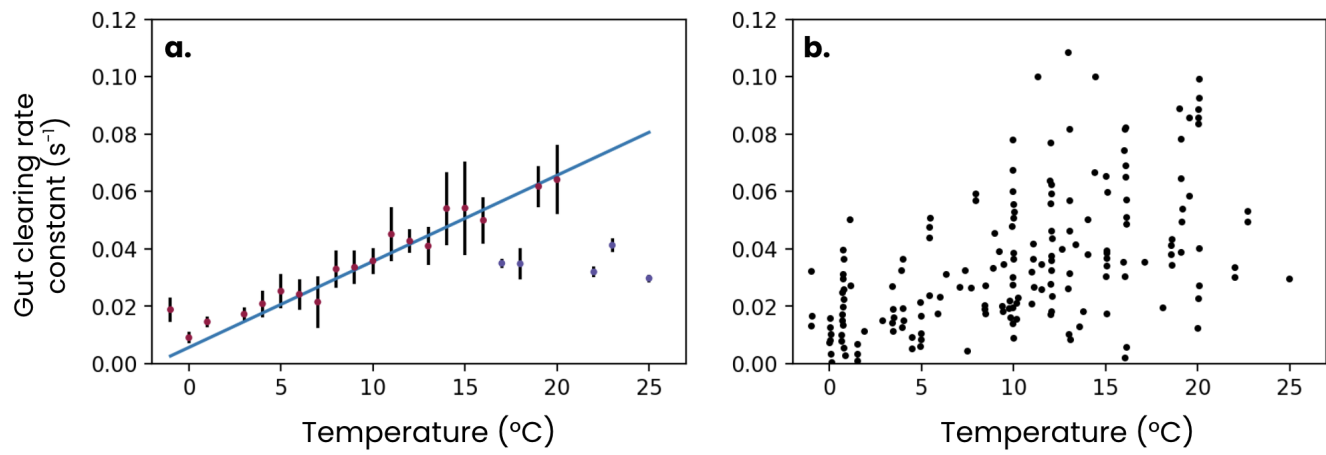
Figure A6. Observations of zooplankton gut clearance rate constant versus temperature, (a) binned for each degree of temperature or (b) raw. Digitised data extracted from Irigoien (1998).
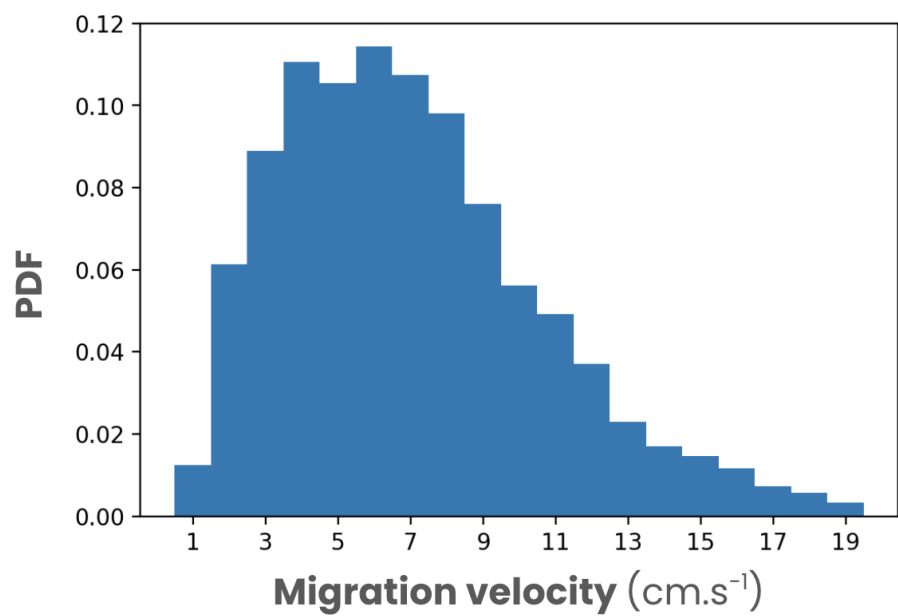
Figure A7. Global distribution of vertical migration velocities of zooplankton measured from global acoustic data by Bianchi and Mislan (2016).
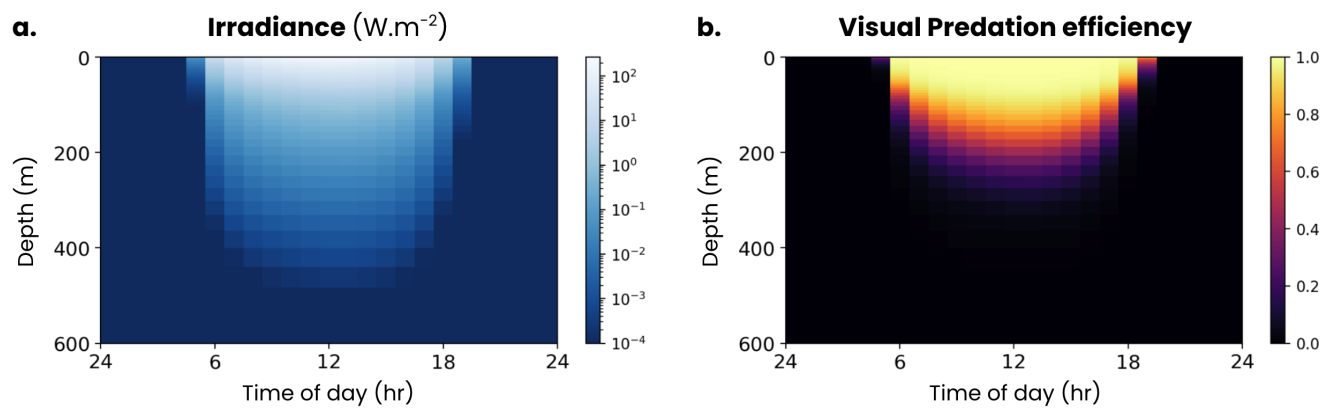
Figure A8. Mean daily cycle of the (a) irradiance and (b) visual predation efficiency vertical distribution in the double gyre model.

Table A1. Major parameters and associated values used in the physical ocean (MOM6) component of the model

Parameter	Spin-Up	Simulation	References
Horizontal grid and resolution	42 x 42, 85 km	362 x 362, 9.4 km	(Adcroft et al. 2019)
Vertical coordinate	45 layer hybrid z^*-isopycnal	75 layer hybrid z^*-isopycnal	
Number of CPUs	60	1024	
Baroclinic and Biogeochemical time steps	1800, 1800 s	300 s, 600 s	
Planetary boundary layer parameterization	ePBL	ePBL	(Reichl and Hallberg. 2018)
Subgrid Mesoscale EKE parameterization	MEKE	No	(Hallberg et al. 2013)
Submesoscale restratification parameterization	No	Frontal length = 1500 m	(Fox-Kemper et al. 2008)
Background kinematic viscosity	$K_V=10^{-4}$ m^2.s^{-1}	$K_V=10^{-6}$ m^2.s^{-1}	
Background diapycnal diffusivity	$K_D=10^{-4}$ m^2.s^{-1}	$K_D=10^{-6}$ m^2.s^{-1}	
Horizontal viscosity	Laplacian ($A_H = 10^5$ m^2.s^{-1}) $A_H = 10^5$ m^2.s^{-1}	Smagorinsky biharmonic Smagorinsky coefficient = 0.015 Resolution-dependent = 0.01 Δ_x^3 m^4 s^{-1}	(Griffies et al. 2000)
Opacity Scheme	3-band with chlorophyll	3-band with chlorophyll	(Manizza et al. 2005)

Appendix B: Results
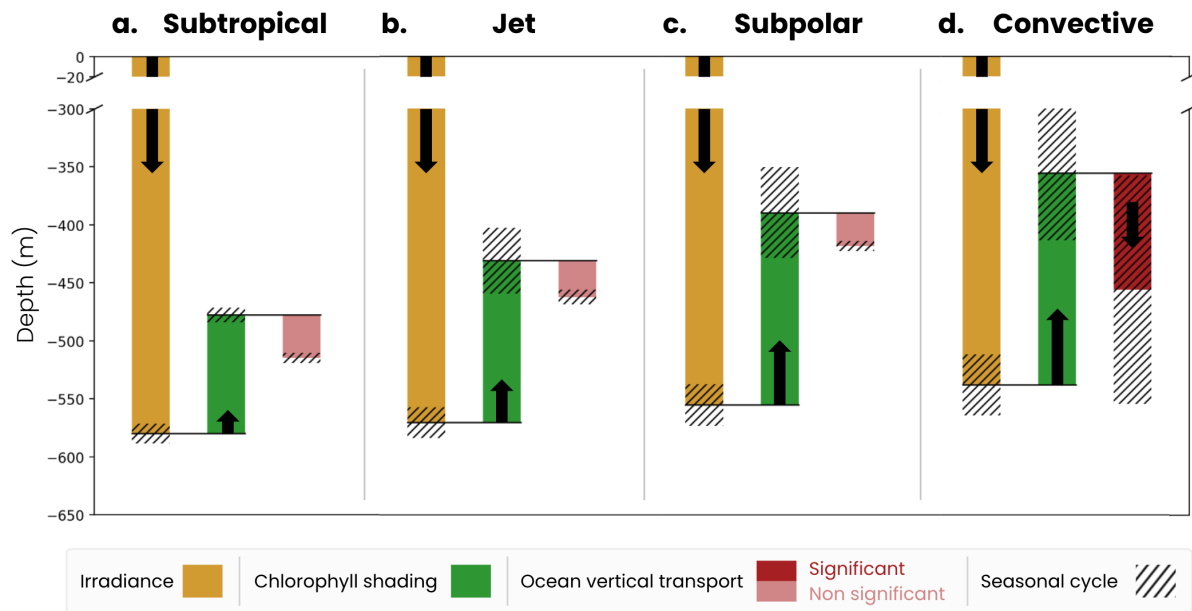
Figure B1. Decomposition of the mechanisms controlling the migration depth of large zooplankton in the (a) subtropical, (b) jet, (c) subpolar and (d) convective biomes. The decomposition includes the effects of large-scale variations in irradiance (yellow bar), chlorophyll shading (green bar) and vertical ocean transport (red bar), and their seasonal range of variability (black hatch). The effect of transport is non-significant (light red bar) when it is smaller than the vertical resolution of the model grid.
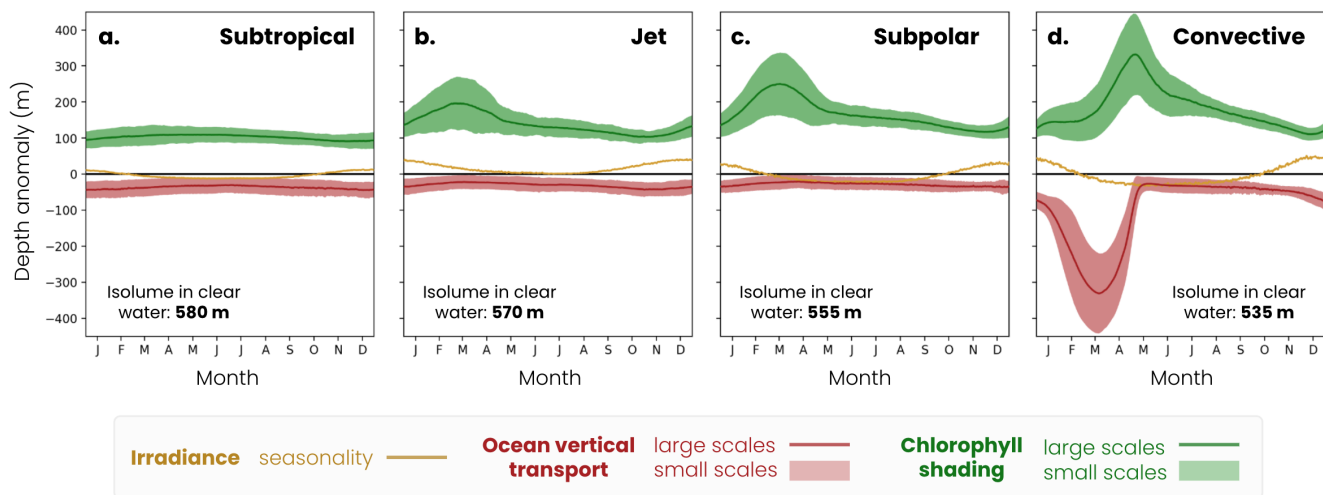
Figure B2. Seasonal decomposition of the mechanisms controlling the medium zooplankton migration depth in (a) the subtropical biome, (b) the jet, (c) the subpolar biome and (d) the convective biome. The lines are the effects of seasonal variations in irradiance (yellow line), large-scale chlorophyll shading (green line) and large-scale vertical transport (red line) relative to a baseline depth set by mean annual irradiance (isolume in clear water, decreasing from 520m in the subpolar gyre to 480m in the convective region). Large-scale effects are superimposed by small-scale spatial variability in chlorophyll shading (green fill) and vertical transport (red fill) induced by eddies and fronts.
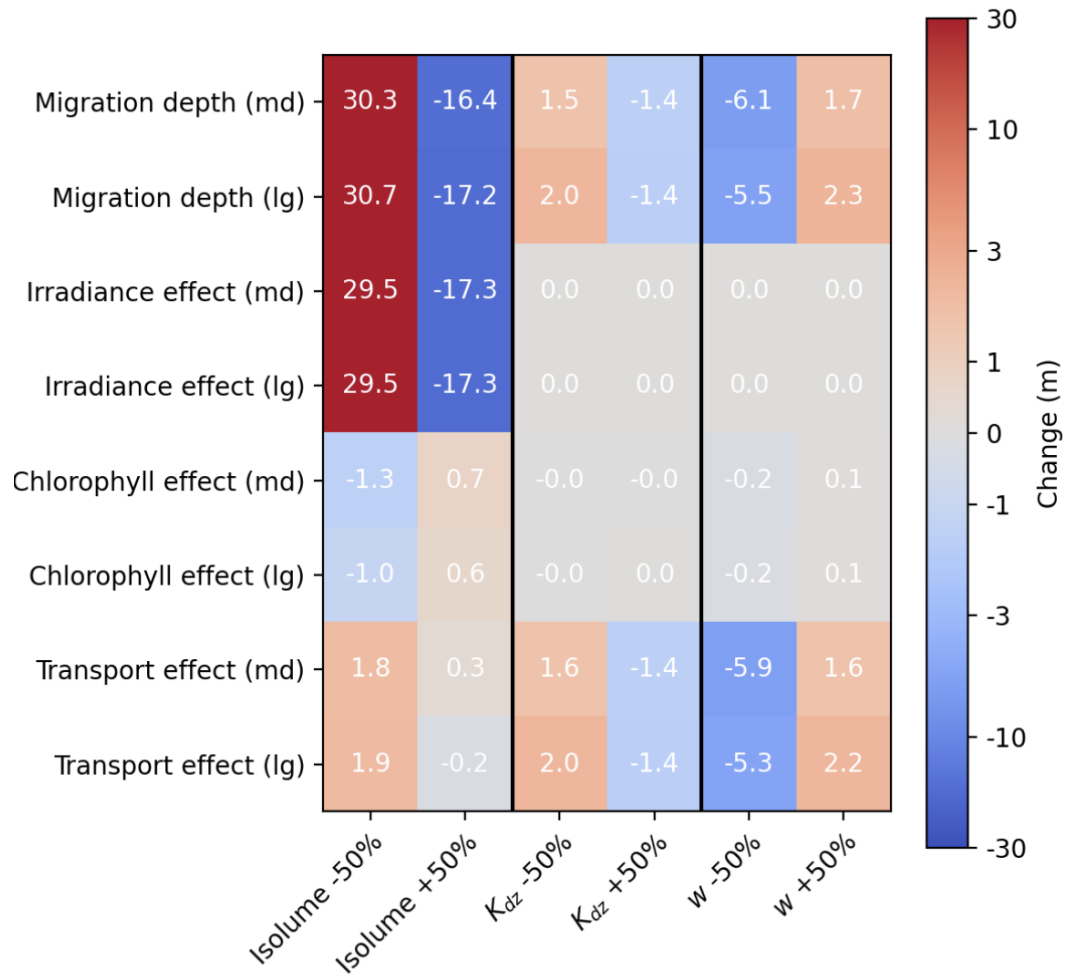
Figure B3. Sensitivity experiment on zooplankton migration depth. Change in migration depth, effect of irradiance, chlorophyll and transport for medium (md) and large (lg) zooplankton in response to a 50% decrease or increase in target isolume, half-saturation distance (K_{dz}) and migration velocity (w). A positive anomaly indicates a deeper migration depth and a negative anomaly a shallower migration depth.

References

Abraham, E. R.: The generation of plankton patchiness by turbulent stirring, Nature, 391, 577–580, https://doi.org/10.1038/35361, number: 6667 Publisher: Nature Publishing Group, 1998.

Adcroft, A., Anderson, W., Balaji, V., Blanton, C., Bushuk, M., Dufour, C. O., Dunne, J. P., Griffies, S. M., Hallberg, R., Harrison, M. J., Held, I. M., Jansen, M. F., John, J. G., Krasting, J. P., Langenhorst, A. R., Legg, S., Liang, Z., McHugh, C., Radhakrishnan, A., Reichl, B. G., Rosati, T., Samuels, B. L., Shao, A., Stouffer, R., Winton, M., Wittenberg, A. T., Xiang, B., Zadeh, N., and Zhang, R.: The GFDL Global Ocean and Sea Ice Model OM4.0: Model Description and Simulation Features, Journal of Advances in Modeling Earth Systems, 11, 3167–3211, https://doi.org/10.1029/2019MS001726, _eprint: https://onlinelibrary.wiley.com/doi/pdf/10.1029/2019MS001726, 2019.

Archibald, K. M., Siegel, D. A., and Doney, S. C.: Modeling the Impact of Zooplankton Diel Vertical Migration on the Carbon Export Flux of the Biological Pump, Global Biogeochemical Cycles, 33, 181–199, https://doi.org/10.1029/2018GB005983, _eprint: https://onlinelibrary.wiley.com/doi/pdf/10.1029/2018GB005983, 2019.

Aumont, O., Maury, O., Lefort, S., and Bopp, L.: Evaluating the Potential Impacts of the Diurnal Vertical Migration by Marine Organisms on Marine Biogeochemistry, Global Biogeochemical Cycles, 32, 1622–1643, https://doi.org/10.1029/2018GB005886, _eprint: https://onlinelibrary.wiley.com/doi/pdf/10.1029/2018GB005886, 2018.

Bandara, K., Varpe, O., Wijewardene, L., Tverberg, V., and Eiane, K.: Two hundred years of zooplankton vertical migration research, Biological Reviews, 96, 1547–1589, https://doi.org/10.1111/brv.12715, _eprint: https://onlinelibrary.wiley.com/doi/pdf/10.1111/brv.12715, 2021.

Barton, A. D., Pershing, A. J., Litchman, E., Record, N. R., Edwards, K. F., Finkel, Z. V., Kiørboe, T., and Ward, B. A.: The biogeography of marine plankton traits, Ecology Letters, 16, 522–534, https://doi.org/10.1111/ele.12063, _eprint: https://onlinelibrary.wiley.com/doi/pdf/10.1111/ele.12063, 2013.

Behrenfeld, M. J. and Falkowski, P. G.: A consumer's guide to phytoplankton primary productivity models, Limnology and Oceanography, 42, 1479–1491, https://doi.org/10.4319/lo.1997.42.7.1479, 1997.

Behrenfeld, M. J., Gaube, P., Della Penna, A., O'Malley, R. T., Burt, W. J., Hu, Y., Bontempi, P. S., Steinberg, D. K., Boss, E. S., Siegel, D. A., Hostetler, C. A., Tortell, P. D., and Doney, S. C.: Global satellite-observed daily vertical migrations of ocean animals, Nature, 576, 257–261, https://doi.org/10.1038/s41586-019-1796-9, number: 7786 Publisher: Nature Publishing Group, 2019.

Beklioglu, M., Gozen, A. G., Yıldırım, F., Zorlu, P., and Onde, S.: Impact of food concentration on diel vertical migration behaviour of Daphnia pulex under fish predation risk, Hydrobiologia, 614, 321–327, https://doi.org/10.1007/s10750-008-9516-8, 2008.

Benoit-Bird, K. J. and Moline, M. A.: Vertical migration timing illuminates the importance of visual and nonvisual predation pressure in the mesopelagic zone, Limnology and Oceanography, 66, 3010–3019, https://doi.org/10.1002/lno.11855, _eprint: https://onlinelibrary.wiley.com/doi/pdf/10.1002/lno.11855, 2021.

Bianchi, D. and Mislan, K. a. S.: Global patterns of diel vertical migration times and velocities from acoustic data, Limnology and Oceanography, 61, 353–364, https://doi.org/10.1002/lno.10219, _eprint: https://onlinelibrary.wiley.com/doi/pdf/10.1002/lno.10219, 2016.

Bianchi, D., Galbraith, E. D., Carozza, D. A., Mislan, K. a. S., and Stock, C. A.: Intensification of open-ocean oxygen depletion by vertically migrating animals, Nature Geoscience, 6, 545–548, https://doi.org/10.1038/ngeo1837, number: 7 Publisher: Nature Publishing Group, 2013a.

Bianchi, D., Stock, C., Galbraith, E. D., and Sarmiento, J. L.: Diel vertical migration: Ecological controls and impacts on the biological pump in a one-dimensional ocean model, Global Biogeochemical Cycles, 27, 478–491, https://doi.org/10.1002/gbc.20031, _eprint: https://onlinelibrary.wiley.com/doi/pdf/10.1002/gbc.20031, 2013b.

Bianchi, D., Babbin, A. R., and Galbraith, E. D.: Enhancement of anammox by the excretion of diel vertical migrators, Proceedings of the National Academy of Sciences, 111, 15 653–15 658, https://doi.org/10.1073/pnas.1410790111, publisher: Proceedings of the National Academy of Sciences, 2014.

Bollens, S. and Frost, B.: Predator-induced diet vertical migration in a planktonic copepod, Journal of Plankton Research, 11, 1047–1065, https://doi.org/10.1093/plankt/11.5.1047, 1989.

Bollens, S. M., Rollwagen-Bollens, G., Quenette, J. A., and Bochdansky, A. B.: Cascading migrations and implications for vertical fluxes in pelagic ecosystems, Journal of Plankton Research, 33, 349–355, https://doi.org/10.1093/plankt/fbq152, 2011.

Boyd, P. W., Claustre, H., Levy, M., Siegel, D. A., and Weber, T.: Multi-faceted particle pumps drive carbon sequestration in the ocean, Nature, 568, 327–335, https://doi.org/10.1038/s41586-019-1098-2, number: 7752 Publisher: Nature Publishing Group, 2019.

Boyer, T. P., García, H. E., Locarnini, R. A., and Zweng, M.: World Ocean Atlas, https://repository.library.noaa.gov/view/noaa/49137, 2018.

Brierley, A. S.: Diel vertical migration, Current biology: CB, 24, R1074–1076, https://doi.org/10.1016/j.cub.2014.08.054, 2014.

Brun, P., Payne, M. R., and Kiørboe, T.: Trait biogeography of marine copepods – an analysis across scales, Ecology Letters, 19, 1403–1413, https://doi.org/10.1111/ele.12688, _eprint: https://onlinelibrary.wiley.com/doi/pdf/10.1111/ele.12688, 2016.

Chambault, P., Teilmann, J., Tervo, O., Sinding, M. H. S., and Heide-Jørgensen, M. P.: The nightscape of the Arctic winter shapes the diving behavior of a marine predator, Scientific Reports, 14, 3908, https://doi.org/10.1038/s41598-024-53953-w, publisher: Nature Publishing Group, 2024.

Cisewski, B., Hátún, H., Kristiansen, I., Hansen, B., Larsen, K. M. H., Eliasen, S. K., and Jacobsen, J. A.: Vertical Migration of Pelagic and Mesopelagic Scatterers From ADCP Backscatter Data in the Southern Norwegian Sea, Frontiers in Marine Science, 7, https://doi.org/10.3389/fmars.2020.542386, publisher: Frontiers, 2021.

Conroy, J. A., Steinberg, D. K., Thibodeau, P. S., and Schofield, O.: Zooplankton diel vertical migration during Antarctic summer, Deep Sea Research Part I: Oceanographic Research Papers, 162, 103 324, https://doi.org/10.1016/j.dsr.2020.103324, 2020.

Cornec, M., Claustre, H., Mignot, A., Guidi, L., Lacour, L., Poteau, A., D'Ortenzio, F., Gentili, B., and Schmechtig, C.: Deep Chlorophyll Maxima in the Global Ocean: Occurrences, Drivers and Characteristics, Global Biogeochemical Cycles, 35, e2020GB006 759, https://doi.org/10.1029/2020GB006759, _eprint: https://onlinelibrary.wiley.com/doi/pdf/10.1029/2020GB006759, 2021.

Couespel, D., Lévy, M., and Bopp, L.: Oceanic primary production decline halved in eddy-resolving simulations of global warming, Biogeosciences, 18, 4321–4349, https://doi.org/10.5194/bg-18-4321-2021, publisher: Copernicus GmbH, 2021.

de Boyer Montégut, C., Madec, G., Fischer, A. S., Lazar, A., and Iudicone, D.: Mixed layer depth over the global ocean: An examination of profile data and a profile-based climatology, Journal of Geophysical Research: Oceans, 109, https://doi.org/10.1029/2004JC002378, _eprint: https://onlinelibrary.wiley.com/doi/pdf/10.1029/2004JC002378, 2004.

Dickson, R. R.: On the Relationship Between Ocean Transparency and the Depth of Sonic Scattering Layers in the North Atlantic, ICES Journal of Marine Science, 34, 416–422, https://doi.org/10.1093/icesjms/34.3.416, 1972.

Dini, M. L. and Carpenter, S. R.: Fish predators, food availability and diel vertical migration in Daphnia, Journal of Plankton Research, 14, 359–377, https://doi.org/10.1093/plankt/14.3.359, 1992.

Dunne, J. P., Horowitz, L. W., Adcroft, A. J., Ginoux, P., Held, I. M., John, J. G., Krasting, J. P., Malyshev, S., Naik, V., Paulot, F., Shevliakova, E., Stock, C. A., Zadeh, N., Balaji, V., Blanton, C., Dunne, K. A., Dupuis, C., Durachta, J., Dussin, R., Gauthier, P. P. G., Griffies, S. M.,

Guo, H., Hallberg, R. W., Harrison, M., He, J., Hurlin, W., McHugh, C., Menzel, R., Milly, P. C. D., Nikonov, S., Paynter, D. J., Ploshay, J., Radhakrishnan, A., Rand, K., Reichl, B. G., Robinson, T., Schwarzkopf, D. M., Sentman, L. T., Underwood, S., Vahlenkamp, H., Winton, M., Wittenberg, A. T., Wyman, B., Zeng, Y., and Zhao, M.: The GFDL Earth System Model Version 4.1 (GFDL-ESM 4.1): Overall Coupled Model Description and Simulation Characteristics, Journal of Advances in Modeling Earth Systems, 12, e2019MS002 015, https://doi.org/10.1029/2019MS002015, _eprint: https://onlinelibrary.wiley.com/doi/pdf/10.1029/2019MS002015, 2020.

Ewald, W. F.: Über Orientierung, Lokomotion und Lichtreaktionen einiger Cladoceren und deren Bedeutung für die Theorie der Tropismen, Buchdruckerei von Junge, google-Books-ID: uFQUAQAAIAAJ, 1910.

Flagg, C. and Smith, S.: Zooplankton Abundance Measurements From Acoustic Doppler Current Profilers, in: Proceedings OCEANS, vol. 5, pp. 1318–1323, https://doi.org/10.1109/OCEANS.1989.587074, 1989.

Flores, H., Veyssière, G., Castellani, G., Wilkinson, J., Hoppmann, M., Karcher, M., Valcic, L., Cornils, A., Geoffroy, M., Nicolaus, M., Niehoff, B., Priou, P., Schmidt, K., and Stroeve, J.: Sea-ice decline could keep zooplankton deeper for longer, Nature Climate Change, pp. 1–9, https://doi.org/10.1038/s41558-023-01779-1, publisher: Nature Publishing Group, 2023.

Garcia, H., Boyer, T., Baranova, O., Locarnini, R., Mishonov, A., Grodsky, A. e., Paver, C., Weathers, K., Smolyar, I., Reagan, J., and others: World ocean atlas 2018: Product documentation, A. Mishonov, Technical Editor, 1, 1–20, 2019.

Gaube, P., McGillicuddy Jr., D. J., Chelton, D. B., Behrenfeld, M. J., and Strutton, P. G.: Regional variations in the influence of mesoscale eddies on near-surface chlorophyll, Journal of Geophysical Research: Oceans, 119, 8195–8220, https://doi.org/10.1002/2014JC010111, _eprint: https://onlinelibrary.wiley.com/doi/pdf/10.1002/2014JC010111, 2014.

Glaholt, S. P., Kennedy, M. L., Turner, E., Colbourne, J. K., and Shaw, J. R.: Thermal variation and factors influencing vertical migration behavior in *Daphnia* populations, Journal of Thermal Biology, 60, 70–78, https://doi.org/10.1016/j.jtherbio.2016.06.008, 2016.

Gonzalez-Pola, C., Larsen, K. M. H., Fratantoni, P., and Beszczynska-Möller, A.: ICES Report on Ocean Climate 2019, report, ICES Cooperative Research Reports (CRR), https://doi.org/10.17895/ices.pub.7537, iSBN: 9788774823100, 2020.

Haren, H. v. and Compton, T. J.: Diel Vertical Migration in Deep Sea Plankton Is Finely Tuned to Latitudinal and Seasonal Day Length, PLOS ONE, 8, e64 435, https://doi.org/10.1371/journal.pone.0064435, publisher: Public Library of Science, 2013.

Harris, J. E.: The Role of Endogenous Rhythms in Vertical Migration, Journal of the Marine Biological Association of the United Kingdom, 43, 153–166, https://doi.org/10.1017/S0025315400005324, 1963.

Hays, G. C.: A review of the adaptive significance and ecosystem consequences of zooplankton diel vertical migrations, Hydrobiologia, 503, 163–170, https://doi.org/10.1023/B:HYDR.0000008476.23617.b0, 2003.

Hays, G. C., Harris, R. P., and Head, R. N.: The vertical nitrogen flux caused by zooplankton diel vertical migration, Marine Ecology Progress Series, 160, 57–62, https://doi.org/10.3354/meps160057, 1997.

Henning, C. C. and Vallis, G. K.: The Effects of Mesoscale Eddies on the Main Subtropical Thermocline, Journal of Physical Oceanography, https://doi.org/10.1175/JPO2639.1, section: Journal of Physical Oceanography, 2004.

Hersbach, H., Bell, B., Berrisford, P., Hirahara, S., Horányi, A., Muñoz-Sabater, J., Nicolas, J., Peubey, C., Radu, R., Schepers, D., Simmons, A., Soci, C., Abdalla, S., Abellan, X., Balsamo, G., Bechtold, P., Biavati, G., Bidlot, J., Bonavita, M., De Chiara, G., Dahlgren, P., Dee, D., Diamantakis, M., Dragani, R., Flemming, J., Forbes, R., Fuentes, M., Geer, A., Haimberger, L., Healy, S., Hogan, R. J., Hólm, E., Janisková, M., Keeley, S., Laloyaux, P., Lopez, P., Lupu, C., Radnoti, G., de Rosnay, P., Rozum, I., Vamborg, F., Villaume, S., and Thépaut, J.-N.: The ERA5 global reanalysis, Quarterly Journal of the Royal Meteorological Society, 146, 1999–2049, https://doi.org/10.1002/qj.3803, _eprint: https://onlinelibrary.wiley.com/doi/pdf/10.1002/qj.3803, 2020.

Hobbs, L., Banas, N. S., Cohen, J. H., Cottier, F. R., Berge, J., and Varpe, O.: A marine zooplankton community vertically structured by light across diel to interannual timescales, Biology Letters, 17, 20200 810, https://doi.org/10.1098/rsbl.2020.0810, publisher: Royal Society, 2021.

Holte, J., Talley, L. D., Gilson, J., and Roemmich, D.: An Argo mixed layer climatology and database, Geophysical Research Letters, 44, 5618–5626, https://doi.org/10.1002/2017GL073426, _eprint: https://onlinelibrary.wiley.com/doi/pdf/10.1002/2017GL073426, 2017.

Irigoien, X.: Gut clearance rate constant, temperature and initial gut contents: a review, Journal of Plankton Research, 20, 997–1003, https://doi.org/10.1093/plankt/20.5.997, 1998.

Jónasdóttir, S. H., Visser, A. W., Richardson, K., and Heath, M. R.: Seasonal copepod lipid pump promotes carbon sequestration in the deep North Atlantic, Proceedings of the National Academy of Sciences, 112, 12 122–12 126, https://doi.org/10.1073/pnas.1512110112, company: National Academy of Sciences Distributor: National Academy of Sciences Institution: National Academy of Sciences Label: National Academy of Sciences Publisher: Proceedings of the National Academy of Sciences, 2015.

Kaiser, P., Hagen, W., von Appen, W.-J., Niehoff, B., Hildebrandt, N., and Auel, H.: Effects of a Submesoscale Oceanographic Filament on Zooplankton Dynamics in the Arctic Marginal Ice Zone, Frontiers in Marine Science, 8, https://doi.org/10.3389/fmars.2021.625395, publisher: Frontiers, 2021.

Kelly, T. B., Davison, P. C., Goericke, R., Landry, M. R., Ohman, M. D., and Stukel, M. R.: The Importance of Mesozooplankton Diel Vertical Migration for Sustaining a Mesopelagic Food Web, Frontiers in Marine Science, 6, https://doi.org/10.3389/fmars.2019.00508, publisher: Frontiers, 2019.

Kimmerer, W. J., Burau, J. R., and Bennett, W. A.: Tidally oriented vertical migration and position maintenance of zooplankton in a temperate estuary, Limnology and Oceanography, 43, 1697–1709, https://doi.org/10.4319/lo.1998.43.7.1697, _eprint: https://onlinelibrary.wiley.com/doi/pdf/10.4319/lo.1998.43.7.1697, 1998.

Klevjer, T. A., Irigoien, X., Røstad, A., Fraile-Nuez, E., Benítez-Barrios, V. M., and Kaartvedt., S.: Large scale patterns in vertical distribution and behaviour of mesopelagic scattering layers, Scientific Reports, 6, 19 873, https://doi.org/10.1038/srep19873, number: 1 Publisher: Nature Publishing Group, 2016.

Kwiatkowski, L., Torres, O., Bopp, L., Aumont, O., Chamberlain, M., Christian, J. R., Dunne, J. P., Gehlen, M., Ilyina, T., John, J. G., Lenton, A., Li, H., Lovenduski, N. S., Orr, J. C., Palmieri, J., Santana-Falcón, Y., Schwinger, J., Séférian, R., Stock, C. A., Tagliabue, A., Takano, Y., Tjiputra, J., Toyama, K., Tsujino, H., Watanabe, M., Yamamoto, A., Yool, A., and Ziehn, T.: Twenty-first century ocean warming, acidification, deoxygenation, and upper-ocean nutrient and primary production decline from CMIP6 model projections, Biogeosciences, 17, 3439–3470, https://doi.org/10.5194/bg-17-3439-2020, publisher: Copernicus GmbH, 2020.

Lass, S. and Spaak, P.: Chemically induced anti-predator defences in plankton: a review, Hydrobiologia, 491, 221–239, https://doi.org/10.1023/A:1024487804497, 2003.

Last, K. S., Hobbs, L., Berge, J., Brierley, A. S., and Cottier, F.: Moonlight Drives Ocean-Scale Mass Vertical Migration of Zooplankton during the Arctic Winter, Current Biology, 26, 244–251, https://doi.org/10.1016/j.cub.2015.11.038, publisher: Elsevier, 2016.

Lehahn, Y., d'Ovidio, F., and Koren, I.: A Satellite-Based Lagrangian View on Phytoplankton Dynamics, Annual Review of Marine Science, 10, 99–119, https://doi.org/10.1146/annurev-marine-121916-063204, 2018.

Llort, J., Langlais, C., Matear, R., Moreau, S., Lenton, A., and Strutton, P. G.: Evaluating Southern Ocean Carbon Eddy-Pump From Biogeochemical-Argo Floats, Journal of Geophysical Research: Oceans, 123, 971–984, https://doi.org/10.1002/2017JC012861, _eprint: https://onlinelibrary.wiley.com/doi/pdf/10.1002/2017JC012861, 2018.

720   Longhurst, A. R. and Glen Harrison, W.: Vertical nitrogen flux from the oceanic photic zone by diel migrant zooplankton and nekton, Deep Sea Research Part A. Oceanographic Research Papers, 35, 881–889, https://doi.org/10.1016/0198-0149(88)90065-9, 1988.

Lévy, M., Jahn, O., Dutkiewicz, S., Follows, M. J., and d'Ovidio, F.: The dynamical landscape of marine phytoplankton diversity, Journal of The Royal Society Interface, 12, 20150 481, https://doi.org/10.1098/rsif.2015.0481, publisher: Royal Society, 2015.

Lévy, M., Franks, P. J. S., and Smith, K. S.: The role of submesoscale currents in structuring marine ecosystems, Nature Communications,
725   9, 4758, https://doi.org/10.1038/s41467-018-07059-3, number: 1 Publisher: Nature Publishing Group, 2018.

Mackas, D. L., Denman, K. L., and Abbott, M. R.: Plankton patchiness: biology in the physical vernacular, Bulletin of Marine Science, 37, 652–674, 1985.

Mahadevan, A.: The Impact of Submesoscale Physics on Primary Productivity of Plankton, Annual Review of Marine Science, 8, 161–184, https://doi.org/10.1146/annurev-marine-010814-015912, _eprint: https://doi.org/10.1146/annurev-marine-010814-015912, 2016.

730   Mangolte, I., Lévy, M., Haëck, C., and Ohman, M. D.: Sub-frontal niches of plankton communities driven by transport and trophic interactions at ocean fronts, Biogeosciences, 20, 3273–3299, https://doi.org/10.5194/bg-20-3273-2023, publisher: Copernicus GmbH, 2023.

Manizza, M., Le Quéré, C., Watson, A. J., and Buitenhuis, E. T.: Bio-optical feedbacks among phytoplankton, upper ocean physics and sea-ice in a global model, Geophysical Research Letters, 32, https://doi.org/10.1029/2004GL020778, _eprint: https://onlinelibrary.wiley.com/doi/pdf/10.1029/2004GL020778, 2005.

735   Marshall, J., Jones, H., Karsten, R., and Wardle, R.: Can Eddies Set Ocean Stratification?, Journal of Physical Oceanography, https://journals.ametsoc.org/view/journals/phoc/32/1/1520-0485_2002_032_0026_cesos_2.0.co_2.xml, section: Journal of Physical Oceanography, 2002.

Martin, A. P.: Phytoplankton patchiness: the role of lateral stirring and mixing, Progress in Oceanography, 57, 125–174, https://doi.org/10.1016/S0079-6611(03)00085-5, 2003.

Martin, A. P., Richards, K. J., Bracco, A., and Provenzale, A.: Patchy productivity in the open ocean, Global Biogeochemical Cycles, 16,
740   9–1–9–9, https://doi.org/10.1029/2001GB001449, _eprint: https://onlinelibrary.wiley.com/doi/pdf/10.1029/2001GB001449, 2002.

McClain, C. R., Franz, B. A., and Werdell, P. J.: Genesis and Evolution of NASA's Satellite Ocean Color Program, Frontiers in Remote Sensing, 3, https://doi.org/10.3389/frsen.2022.938006, publisher: Frontiers, 2022.

Michael, E. L. R.: Classification and vertical distribution of the Chaetognatha of the San Diego region, including redescriptions of some doubtful species of the group, University of California publications in zoology, The University Press, Berkeley, oCLC: 2806752, 1911.

745   Nocera, A. C., Dumont, D., and Schloss, I. R.: A zooplankton diel vertical migration parameterization for coastal marine ecosystem modeling, Biogeosciences Discussions, pp. 1–21, https://doi.org/10.5194/bg-2020-10, publisher: Copernicus GmbH, 2020.

Notz, D. and Community, S.: Arctic Sea Ice in CMIP6, Geophysical Research Letters, 47, e2019GL086 749, https://doi.org/10.1029/2019GL086749, _eprint: https://onlinelibrary.wiley.com/doi/pdf/10.1029/2019GL086749, 2020.

Nowicki, M., DeVries, T., and Siegel, D. A.: Quantifying the Carbon Export and Sequestration Pathways of the Ocean's Bi-
750   ological Carbon Pump, Global Biogeochemical Cycles, 36, e2021GB007 083, https://doi.org/10.1029/2021GB007083, _eprint: https://onlinelibrary.wiley.com/doi/pdf/10.1029/2021GB007083, 2022.

Ohman, M. D. and Romagnan, J.-B.: Nonlinear effects of body size and optical attenuation on Diel Vertical Migration by zooplankton, Limnology and Oceanography, 61, 765–770, https://doi.org/10.1002/lno.10251, _eprint: https://onlinelibrary.wiley.com/doi/pdf/10.1002/lno.10251, 2016.

755   Ohman, M. D., Frost, B. W., and Cohen, E. B.: Reverse Diel Vertical Migration: An Escape from Invertebrate Predators, Science, 220, 1404–1407, https://doi.org/10.1126/science.220.4604.1404, publisher: American Association for the Advancement of Science, 1983.

Olsen, A., Lange, N., Key, R. M., Tanhua, T., Bittig, H. C., Kozyr, A., Álvarez, M., Azetsu-Scott, K., Becker, S., Brown, P. J., Carter, B. R., Cotrim da Cunha, L., Feely, R. A., van Heuven, S., Hoppema, M., Ishii, M., Jeansson, E., Jutterström, S., Landa, C. S., Lauvset, S. K., Michaelis, P., Murata, A., Pérez, F. F., Pfeil, B., Schirnick, C., Steinfeldt, R., Suzuki, T., Tilbrook, B., Velo, A., Wanninkhof, R., and Woosley, R. J.: An updated version of the global interior ocean biogeochemical data product, GLODAPv2.2020, Earth System Science Data, 12, 3653–3678, https://doi.org/10.5194/essd-12-3653-2020, publisher: Copernicus GmbH, 2020.

Omand, M. M., Steinberg, D. K., and Stamieszkin, K.: Cloud shadows drive vertical migrations of deep-dwelling marine life, Proceedings of the National Academy of Sciences, 118, e2022977 118, https://doi.org/10.1073/pnas.2022977118, publisher: Proceedings of the National Academy of Sciences, 2021.

Petrusevich, V., Dmitrenko, I. A., Kirillov, S. A., Rysgaard, S., Falk-Petersen, S., Barber, D. G., Boone, W., and Ehn, J. K.: Wintertime water dynamics and moonlight disruption of the acoustic backscatter diurnal signal in an ice-covered Northeast Greenland fjord, Journal of Geophysical Research: Oceans, 121, 4804–4818, https://doi.org/10.1002/2016JC011703, _eprint: https://onlinelibrary.wiley.com/doi/pdf/10.1002/2016JC011703, 2016.

Pijanowska, J. and Dawidowicz, P.: The lack of vertical migration in Daphnia: the effect of homogenously distributed food, Hydrobiologia, 148, 175–181, https://doi.org/10.1007/BF00008403, 1987.

Pinti, J., Kiørboe, T., Thygesen, U. H., and Visser, A. W.: Trophic interactions drive the emergence of diel vertical migration patterns: a game-theoretic model of copepod communities, Proceedings of the Royal Society B: Biological Sciences, 286, 20191 645, https://doi.org/10.1098/rspb.2019.1645, publisher: Royal Society, 2019.

Piron, A., Thierry, V., Mercier, H., and Caniaux, G.: Gyre-scale deep convection in the subpolar North Atlantic Ocean during winter 2014–2015, Geophysical Research Letters, 44, 1439–1447, https://doi.org/10.1002/2016GL071895, _eprint: https://onlinelibrary.wiley.com/doi/pdf/10.1002/2016GL071895, 2017.

Powell, J. R. and Ohman, M. D.: Covariability of zooplankton gradients with glider-detected density fronts in the Southern California Current System, Deep Sea Research Part II: Topical Studies in Oceanography, 112, 79–90, https://doi.org/10.1016/j.dsr2.2014.04.002, 2015.

Press, W. H.: Numerical Recipes 3rd Edition: The Art of Scientific Computing, Cambridge University Press, ISBN 978-0-521-88068-8, google-Books-ID: 1aAOdzK3FegC, 2007.

Radko, T. and Marshall, J.: Equilibration of a Warm Pumped Lens on a b plane, Journal of Physical Oceanography, https://journals.ametsoc.org/view/journals/phoc/33/4/1520-0485_2003_33_885_eoawpl_2.0.co_2.xml, section: Journal of Physical Oceanography, 2003.

Resplandy, L., Martin, A. P., Le Moigne, F., Martin, P., Aquilina, A., Mémery, L., Lévy, M., and Sanders, R.: How does dynamical spatial variability impact 234Th-derived estimates of organic export?, Deep Sea Research Part I: Oceanographic Research Papers, 68, 24–45, https://doi.org/10.1016/j.dsr.2012.05.015, 2012.

Resplandy, L., Lévy, M., and McGillicuddy Jr., D. J.: Effects of Eddy-Driven Subduction on Ocean Biological Carbon Pump, Global Biogeochemical Cycles, 33, 1071–1084, https://doi.org/10.1029/2018GB006125, _eprint: https://onlinelibrary.wiley.com/doi/pdf/10.1029/2018GB006125, 2019.

Riquelme-Bugueño, R., Pérez-Santos, I., Alegría, N., Vargas, C. A., Urbina, M. A., and Escribano, R.: Diel vertical migration into anoxic and high-pCO2 waters: acoustic and net-based krill observations in the Humboldt Current, Scientific Reports, 10, 17 181, https://doi.org/10.1038/s41598-020-73702-z, publisher: Nature Publishing Group, 2020.

Russell, F. S.: The Vertical Distribution of Plankton in the Sea, Biological Reviews, 2, 213–262, https://doi.org/10.1111/j.1469-185X.1927.tb00878.x, _eprint: https://onlinelibrary.wiley.com/doi/pdf/10.1111/j.1469-185X.1927.tb00878.x, 1927.

Sathyendranath, S., Brewin, R. J. W., Brockmann, C., Brotas, V., Calton, B., Chuprin, A., Cipollini, P., Couto, A. B., Dingle, J., Doerffer, R., Donlon, C., Dowell, M., Farman, A., Grant, M., Groom, S., Horseman, A., Jackson, T., Krasemann, H., Lavender, S., Martinez-Vicente, V., Mazeran, C., Mélin, F., Moore, T. S., Müller, D., Regner, P., Roy, S., Steele, C. J., Steinmetz, F., Swinton, J., Taberner, M., Thompson, A., Valente, A., Zühlke, M., Brando, V. E., Feng, H., Feldman, G., Franz, B. A., Frouin, R., Gould, R. W., Hooker, S. B., Kahru, M., Kratzer, S., Mitchell, B. G., Muller-Karger, F. E., Sosik, H. M., Voss, K. J., Werdell, J., and Platt, T.: An Ocean-Colour Time Series for Use in Climate Studies: The Experience of the Ocean-Colour Climate Change Initiative (OC-CCI), Sensors, 19, 4285, https://doi.org/10.3390/s19194285, number: 19 Publisher: Multidisciplinary Digital Publishing Institute, 2019.

Sgubin, G., Swingedouw, D., Drijfhout, S., Mary, Y., and Bennabi, A.: Abrupt cooling over the North Atlantic in modern climate models, Nature Communications, 8, 14 375, https://doi.org/10.1038/ncomms14375, publisher: Nature Publishing Group, 2017.

Silsbe, G. M., Behrenfeld, M. J., Halsey, K. H., Milligan, A. J., and Westberry, T. K.: The CAFE model: A net production model for global ocean phytoplankton, Global Biogeochemical Cycles, 30, 1756–1777, https://doi.org/10.1002/2016GB005521, 2016.

Steinberg, D. K., Carlson, C. A., Bates, N. R., Goldthwait, S. A., Madin, L. P., and Michaels, A. F.: Zooplankton vertical migration and the active transport of dissolved organic and inorganic carbon in the Sargasso Sea, Deep Sea Research Part I: Oceanographic Research Papers, 47, 137–158, https://doi.org/10.1016/S0967-0637(99)00052-7, 2000.

Steinberg, D. K., Goldthwait, S. A., and Hansell, D. A.: Zooplankton vertical migration and the active transport of dissolved organic and inorganic nitrogen in the Sargasso Sea, Deep Sea Research Part I: Oceanographic Research Papers, 49, 1445–1461, https://doi.org/10.1016/S0967-0637(02)00037-7, 2002.

Steinberg, D. K., Cope, J. S., Wilson, S. E., and Kobari, T.: A comparison of mesopelagic mesozooplankton community structure in the subtropical and subarctic North Pacific Ocean, Deep Sea Research Part II: Topical Studies in Oceanography, 55, 1615–1635, https://doi.org/10.1016/j.dsr2.2008.04.025, 2008.

Steinberg, D. K., Lomas, M. W., and Cope, J. S.: Long-term increase in mesozooplankton biomass in the Sargasso Sea: Linkage to climate and implications for food web dynamics and biogeochemical cycling, Global Biogeochemical Cycles, 26, https://doi.org/10.1029/2010GB004026, _eprint: https://onlinelibrary.wiley.com/doi/pdf/10.1029/2010GB004026, 2012.

Stock, C. A., Dunne, J. P., and John, J. G.: Global-scale carbon and energy flows through the marine planktonic food web: An analysis with a coupled physical–biological model, Progress in Oceanography, 120, 1–28, https://doi.org/10.1016/j.pocean.2013.07.001, 2014.

Stock, C. A., Dunne, J. P., Fan, S., Ginoux, P., John, J., Krasting, J. P., Laufkötter, C., Paulot, F., and Zadeh, N.: Ocean Biogeochemistry in GFDL's Earth System Model 4.1 and Its Response to Increasing Atmospheric CO2, Journal of Advances in Modeling Earth Systems, 12, e2019MS002 043, https://doi.org/10.1029/2019MS002043, _eprint: https://onlinelibrary.wiley.com/doi/pdf/10.1029/2019MS002043, 2020.

Strömberg, J.-O., Spicer, J. I., Liljebladh, B., and Thomasson, M. A.: Northern krill, Meganyctiphanes norvegica, come up to see the last eclipse of the millennium?, Journal of the Marine Biological Association of the United Kingdom, 82, 919–920, https://doi.org/10.1017/S0025315402006367, 2002.

Torres, J. J. and Childress, J. J.: Relationship of oxygen consumption to swimming speed in Euphausiapacifica, Marine Biology, 1983.

Tsujino, H., Urakawa, S., Nakano, H., Small, R. J., Kim, W. M., Yeager, S. G., Danabasoglu, G., Suzuki, T., Bamber, J. L., Bentsen, M., Böning, C. W., Bozec, A., Chassignet, E. P., Curchitser, E., Boeira Dias, F., Durack, P. J., Griffies, S. M., Harada, Y., Ilicak, M., Josey, S. A., Kobayashi, C., Kobayashi, S., Komuro, Y., Large, W. G., Le Sommer, J., Marsland, S. J., Masina, S., Scheinert, M., Tomita, H., Valdivieso, M., and Yamazaki, D.: JRA-55 based surface dataset for driving ocean–sea-ice models (JRA55-do), Ocean Modelling, 130, 79–139, https://doi.org/10.1016/j.ocemod.2018.07.002, 2018.

Vignesh, P. P., Jiang, J. H., Kishore, P., Su, H., Smay, T., Brighton, N., and Velicogna, I.: Assessment of CMIP6 Cloud Fraction and Comparison with Satellite Observations, Earth and Space Science, 7, e2019EA000 975, https://doi.org/10.1029/2019EA000975, _eprint: https://onlinelibrary.wiley.com/doi/pdf/10.1029/2019EA000975, 2020.

835 Våge, K., Pickart, R. S., Thierry, V., Reverdin, G., Lee, C. M., Petrie, B., Agnew, T. A., Wong, A., and Ribergaard, M. H.: Surprising return of deep convection to the subpolar North Atlantic Ocean in winter 2007–2008, Nature Geoscience, 2, 67–72, https://doi.org/10.1038/ngeo382, publisher: Nature Publishing Group, 2009.

Westberry, T., Behrenfeld, M. J., Siegel, D. A., and Boss, E.: Carbon-based primary productivity modeling with vertically resolved photoacclimation, Global Biogeochemical Cycles, 22, 2007GB003 078, https://doi.org/10.1029/2007GB003078, 2008.

840 Zaret, T. M. and Suffern, J. S.: Vertical migration in zooplankton as a predator avoidance mechanism1, Limnology and Oceanography, 21, 804–813, https://doi.org/10.4319/lo.1976.21.6.0804, _eprint: https://onlinelibrary.wiley.com/doi/pdf/10.4319/lo.1976.21.6.0804, 1976.